



**UNIVERSITY  
OF TURKU**

# **PET IMAGING OF ISCHAEMIC MYOCARDIAL INJURY AND ANGIOGENESIS**

**Maria Grönman**





UNIVERSITY  
OF TURKU

# **PET IMAGING OF ISCHAEMIC MYOCARDIAL INJURY AND ANGIOGENESIS**

---

Maria Grönman

## University of Turku

---

Faculty of Medicine  
Clinical Physiology and Isotope Medicine  
Drug Research Doctoral programme  
Turku PET Centre

## Supervised by

---

Professor, Anne Roivainen  
Turku PET Centre and Turku Center for  
Disease Modeling  
University of Turku  
Turku, Finland

Professor, Antti Saraste  
Turku PET Centre, Heart Center and  
Institute of Clinical Medicine  
University of Turku and Turku University  
Hospital, Turku, Finland

## Reviewed by

---

Adjunct Professor, Riikka Kivelä  
Stem Cells and Metabolism Research  
Program  
University of Helsinki  
Helsinki, Finland

Adjunct Professor, Jens Sörensen  
Department of Surgical Sciences,  
Radiology  
Uppsala University  
Akademiska sjukhuset  
Uppsala, Sweden

## Opponent

---

Professor, Tomi Laitinen  
Clinical Physiology and Nuclear  
Medicine  
University of Eastern Finland  
Kuopio, Finland

The originality of this publication has been checked in accordance with the University of Turku quality assurance system using the Turnitin OriginalityCheck service.

ISBN 978-951-29-8156-4 (PRINT)  
ISBN 978-951-29-8157-1 (PDF)  
ISSN 0355-9483 (Print)  
ISSN 2343-3213 (Online)  
Painosalama, Turku, Finland 2020

*Tietä käyden tien on vanki, vapaa on vain umpihanki*

– Aaro Hellaakoski

UNIVERSITY OF TURKU

Faculty of Medicine

Clinical Physiology and Isotope Medicine

MARIA GRÖNMAN: PET Imaging of Ischaemic Myocardial Injury and

Angiogenesis

Doctoral Dissertation, 111 pp.

Drug Research Doctoral Programme

September 2020

## ABSTRACT

The myocardium of patients with coronary artery disease (CAD) often is a mixture of ischaemic but viable tissue and irreversibly injured scar tissue. The viable tissue has capability of functional recovery after restoration of blood flow and the assessment of myocardial viability is important in identifying patients who will most likely benefit from revascularisation. Angiogenesis is an essential part of the healing process after ischaemic myocardial injury aiming at restoration of intact tissue capillary network. Measurement of myocardial blood flow by positron emission tomography (PET) and [<sup>15</sup>O]water is widely used in the evaluation of CAD, but its value in the assessment of myocardial viability is incompletely understood. [<sup>68</sup>Ga]NODAGA-RGD is a novel PET tracer binding to  $\alpha_v\beta_3$  integrin that plays a central role in angiogenesis and therefore, may enable imaging of angiogenic activity.

The purpose of this thesis was to evaluate [<sup>15</sup>O]water and [<sup>68</sup>Ga]NODAGA-RGD for the assessment of myocardial viability and ischaemic myocardial injury by PET in experimental models. We used pig models of surgically or percutaneously induced coronary stenosis and human cell based *in vitro* model of angiogenesis. In the first substudy, we found that resting myocardial blood flow (MBF), perfusable tissue fraction (PTF) and perfusable tissue index (PTI) by [<sup>15</sup>O]water PET detected myocardial viability with good accuracy in pig models of ischaemic heart failure and myocardial ischaemia. In the second substudy, we found that [<sup>68</sup>Ga]NODAGA-RGD demonstrated increased myocardial  $\alpha_v\beta_3$  integrin expression in the ischaemic myocardium that was localised in the irreversibly injured myocardium. In the third substudy, we found that the uptake of [<sup>68</sup>Ga]NODAGA-RGD was proportional to angiogenic activity in an *in vitro* angiogenesis tissue model.

In conclusion, these experimental studies indicate that resting MBF, PTF and PTI by [<sup>15</sup>O]water PET are useful indexes of myocardial viability in chronic CAD. [<sup>68</sup>Ga]NODAGA-RGD PET may be useful for the identification of  $\alpha_v\beta_3$  integrin activation associated with recent ischaemic myocardial injury. This tracer reflects angiogenetic activity *in vitro*, but its specificity for angiogenesis *in vivo* remains uncertain.

**KEYWORDS:** Coronary artery disease, myocardial infarction, myocardial viability, angiogenesis, positron emission tomography

TURUN YLIOPISTO

Lääketieteellinen tiedekunta

Kliininen fysiologia ja isotooppilääketiede

MARIA GRÖNMAN: Sydänlihaksen iskeemisen vaurion ja uudisverisuonituksen PET kuvantaminen

Väitöskirja, 111 s.

Lääketutkimuksen tohtoriohjelma

September 2020

## TIIVISTELMÄ

Sepelvaltimotautipotilaiden sydänlihas koostuu usein iskeemisestä, mutta elinkykyisestä ja peruuttamattomasti vaurioituneesta kudoksesta. Elinakykyisen sydänlihaksen toiminta voi palautua normaalisti verenkierron palauttamisen jälkeen, ja elinkykyisyyden arviointi on tärkeää verenkierron palauttamisesta hyötyvien potilaiden tunnistamisessa. Uudisverisuonitus eli angiogeneesi, jonka tarkoitus on palauttaa kudokseen toimiva hiussuoniverkosto, on tärkeä osa iskeemisen vaurion jälkeistä paranemista. Sydänlihaksen verenvirtauksen mittaaminen positroniemissiotomografialla (PET) käyttäen merkkiaineena [<sup>15</sup>O]vettä on paljon käytetty menetelmä sydäntaudin arvioinnissa, mutta sen soveltuvuutta sydänlihaksen elinkykyisyyden arviointiin ei tiedetä. [<sup>68</sup>Ga]NODAGA-RGD on uusi angiogeneesiä säätelevään  $\alpha_v\beta_3$  integriiniin sitoutuva merkkiaine jonka avulla voitaisi mahdollisesti kuvantaa sydänlihaksen angiogeenistä aktiivisuutta.

Väitöskirjatyon tarkoituksena oli arvioida [<sup>15</sup>O]vesi ja [<sup>68</sup>Ga]NODAGA-RGD PET:n käyttökelpoisuutta sydänlihaksen elinkykyisyyden ja iskeemisen sydänlihaskudoksen tunnistamisessa kokeellisilla malleilla. Käytimme sikoja, joille oli aiheutettu sepelvaltimotukos kirurgisesti tai katetrisaatiolla, sekä ihmislupohjaista kokeellista angiogeenin kudomallia. Ensimmäisessä osatyössä havaitsimme, että [<sup>15</sup>O]vesi PET:n tehokkuus elinkykyisyyden havaitsemisessa iskeemisen sydämen vajaatoiminnan ja sydänlihaskemian sikamalleissa oli hyvä. Toisessa osatyössä havaitsimme, että [<sup>68</sup>Ga]NODAGA-RGD:llä voitiin havaita lisääntynyt  $\alpha_v\beta_3$  integriiniaktivaatio, joka sijaitti peruuttamattomasti vaurioituneessa sydänlihaksessa. Kolmannessa osatyössä havaitsimme, että [<sup>68</sup>Ga]NODAGA-RGD:n kertymä oli verrannollinen angiogeneesiaktivaatioon kokeellisessa angiogeenin kudomallissa.

Yhteenvetona voidaan todeta, että [<sup>15</sup>O]vesi PET on käyttökelpoinen sydänlihaksen elinkykyisyyden arvioinnissa kroonisessa sepelvaltimotaudissa. [<sup>68</sup>Ga]NODAGA-RGD PET voi olla käyttökelpoinen tuoreeseen sydänlihaskudon vaurioon liittyvän  $\alpha_v\beta_3$  integriiniaktivaation kuvantamisessa. Tämä merkkiaine kuvastaa angiogeenistä aktivaatiota kokeellisesti, mutta sen tarkkuus elävissä elimistössä on epäselvää.

AVAINSANAT: Sepelvaltimotauti, sydäninfarkti, sydänlihaksen elinkykyisyys, uudisverisuonitus, positroniemissiotomografia

# Table of Contents

<b>Abbreviations .....</b>	<b>8</b>
<b>List of Original Publications .....</b>	<b>10</b>
<b>1 Introduction .....</b>	<b>11</b>
<b>2 Review of the Literature .....</b>	<b>13</b>
2.1 Ischaemic heart disease.....	13
2.1.1 Coronary artery disease .....	13
2.1.2 Myocardial ischaemia and infarction.....	13
2.1.3 Healing after myocardial infarction .....	14
2.1.3.1 Inflammatory phase .....	15
2.1.3.2 Proliferative phase .....	15
2.1.3.3 Maturation phase .....	18
2.1.3.4 Adverse remodelling and heart failure .....	19
2.1.4 Myocardial viability .....	21
2.2 Pig as an experimental model of chronic myocardial ischaemia.....	22
2.3 Myocardial perfusion imaging in ischaemic heart disease .....	23
2.3.1 Myocardial perfusion imaging with PET .....	24
2.4 Imaging of myocardial viability.....	27
2.4.1 SPECT .....	27
2.4.2 PET .....	28
2.4.3 Echocardiography .....	28
2.4.4 Cardiac magnetic resonance imaging .....	29
2.5 PET imaging of myocardial injury and angiogenesis .....	30
2.5.1 Inflammation .....	30
2.5.2 Angiogenesis .....	31
2.5.3 Fibrosis .....	31
<b>3 Aims .....</b>	<b>33</b>
<b>4 Materials and Methods .....</b>	<b>34</b>
4.1 Animal models (I, II) .....	34
4.1.1 Study outline (I, II) .....	34
4.1.2 Anaesthesia and hemodynamic monitoring .....	34
4.1.3 Bottleneck stent model for myocardial ischaemia (I, II) .....	35
4.1.4 Ameroid model (I).....	35
4.2 <i>In vivo</i> PET studies .....	36



4.2.1	Imaging myocardial perfusion with [ <sup>15</sup> O]water PET (I, II).....	36
4.2.2	Imaging integrin expression with [ <sup>68</sup> Ga]NODAGA-RGD (II).....	37
4.2.3	PET image analyses .....	37
4.3	Tissue analyses .....	39
4.3.1	TTC (I, II).....	39
4.3.2	<i>Ex vivo</i> autoradiography (II).....	39
4.3.3	<i>Ex vivo</i> biodistribution (II) .....	39
4.3.4	Histology and immunohistochemistry (II) .....	40
4.3.4.1	General histology.....	40
4.3.4.2	Immunohistochemical stainings of CD31, $\alpha_v\beta_3$ integrin and $\alpha$ -SMA.....	40
4.4	<i>In vitro</i> experiments .....	40
4.4.1	Plasma protein binding (II).....	40
4.4.2	Angiogenesis tissue model (III).....	40
4.4.3	<i>In vitro</i> receptor binding (III).....	41
4.4.4	<i>In vitro</i> autoradiography (III).....	41
4.4.5	Immunohistochemical stainings (III).....	41
4.5	Statistical analysis .....	41
<b>5</b>	<b>Results .....</b>	<b>43</b>
5.1	Imaging of myocardial blood flow and viability (I).....	43
5.1.1	MBF and PTF in MI .....	43
5.1.2	Detection of infarction.....	43
5.1.3	Assessment of viability .....	44
5.2	Imaging of myocardial injury and angiogenesis (II and III) .....	46
5.2.1	[ <sup>68</sup> Ga]NODAGA-RGD <i>in vivo</i> PET.....	46
5.2.2	Histology .....	46
5.2.3	<i>Ex vivo</i> experiments .....	47
5.2.3.1	Biodistribution .....	47
5.2.3.2	Autoradiography .....	47
5.2.4	<i>In vitro</i> experiments .....	47
5.2.4.1	<i>In vitro</i> tracer binding .....	47
5.2.4.2	Autoradiography .....	48
<b>6</b>	<b>Discussion .....</b>	<b>49</b>
6.1	Pig models of myocardial ischaemia and infarction .....	49
6.2	Imaging of myocardial blood flow and viability .....	50
6.3	Imaging of myocardial injury and angiogenesis .....	52
6.4	Future directions .....	54
<b>7</b>	<b>Conclusions.....</b>	<b>56</b>
	<b>Acknowledgements .....</b>	<b>57</b>
	<b>References .....</b>	<b>61</b>
	<b>Original Publications.....</b>	<b>75</b>

# Abbreviations

ACE	Angiotensin-converting enzyme
AT	Angiotensin
AT1R	Angiotensin II subtype 1 receptor
ATF	Anatomical tissue fraction
ATP	Adenosine triphosphate
AUC	Area under the curve
CAD	Coronary artery disease
CMR	Cardiac magnetic resonance
CT	Computed tomography
cTN	Cardiac troponin
DAMP	Danger-associated molecular pattern
ECG	Electrocardiogram
ECM	Extracellular matrix
EDWT	End diastolic wall thickness
FDG	Fluorodeoxyglucose
FGF	Fibroblast growth factor
GLUT	Glucose transporter
GMP	Good manufacturing practice
hASC	Human adipose stromal cells
HF	Heart failure
HIF	Hypoxia-inducible factor
HMGB1	High mobility group box 1
HSP	Heat shock protein
HUVEC	Human umbilical vein endothelial cells
IAP	Inhibitor of apoptosis
IHD	Ischaemic heart disease
IL	Interleukin
LAD	Left anterior descending artery
LV	Left ventricle
MI	Myocardial infarction
MBF	Myocardial blood flow

MPI	Myocardial perfusion imaging
MRI	Magnetic resonance imaging
PBS	Phosphate-buffered saline
PET	Positron emission tomography
PSL	Photostimulated luminescence
PTF	Perfusable tissue fraction
PTI	Perfusable tissue index
RAAS	Renin-angiotensin-aldosterone system
RGD	Arginine-glycine-aspartic acid
ROC	Receiver operating characteristics
ROI	Region of interest
ROS	Reactive oxygen species
SMA	Smooth muscle actin
SPECT	Single photon emission computed tomography
SUV	Standardised uptake value
TGF	Transforming growth factor
TLR	Toll-like receptor
TNF	Tumor necrosis factor
TTC	2,3,5-triphenyltetrazolium chloride
VEGF	Vascular endothelial growth factor
VOI	Volume of interest
vWF	von Willebrand factor

# List of Original Publications

This dissertation is based on the following original publications, which are referred to in the text by their Roman numerals:

- I Maria Grönman, Miikka Tarkia, Christoffer Stark, Tommi Vähäsilta, Tuomas Kiviniemi, Mark Lubberink, Paavo Halonen, Antti Kuivanen, Virva Saunavaara, Tuula Tolvanen, Jarmo Teuvo, Mika Teräs, Timo Savunen, Mikko Pietilä, Seppo Ylä-Herttua, Anne Roivainen, Juhani Knuuti, Antti Saraste. Assessment of myocardial viability with [<sup>15</sup>O]water PET: A validation study in experimental myocardial infarction. *Journal of Nuclear Cardiology*. (2019). <https://doi.org/10.1007/s12350-019-01818-5>.
- II Maria Grönman, Miikka Tarkia, Tuomas Kiviniemi, Paavo Halonen, Antti Kuivanen, Timo Savunen, Tuula Tolvanen, Jarmo Teuvo, Meeri Käkelä, Olli Metsälä, Mikko Pietilä, Pekka Saukko, Seppo Ylä-Herttua, Juhani Knuuti, Anne Roivainen, Antti Saraste. Imaging of  $\alpha_v\beta_3$  integrin expression in experimental myocardial ischemia with [<sup>68</sup>Ga]NODAGA-RGD positron emission tomography. *Journal of Translational Medicine*, 2017; 15: 144.
- III Maria Grönman, Olli Moisio, Xiang-Guo Li, Tarja Toimela, Outi Huttala, Tuula Heinonen, Juhani Knuuti, Anne Roivainen, Antti Saraste. Association between [<sup>68</sup>Ga]NODAGA-RGDyK uptake and dynamics of angiogenesis in a human cell-based 3D model. *Manuscript submitted for publication*

The original publications have been reproduced with the permission of the copyright holders.

# 1 Introduction

Ischaemic heart disease (IHD) is the leading global cause of death (Moran et al., 2014). It is caused by atherosclerosis of the coronary arteries and can also be called coronary artery disease (CAD). The atherosclerotic plaques start to develop early and slowly progress to narrow the artery lumen, reduce the myocardial blood flow (MBF) and cause myocardial ischemia. The myocardium of patients with CAD and left ventricle (LV) dysfunction often contains a mixture of ischemic, but viable and irreversibly injured, non-viable tissue. The viable tissue still has capability of regaining contractile function after the restoration of blood flow, whereas non-viable tissue does not benefit from revascularisation (Bax & Delgado, 2015). Myocardial perfusion imaging (MPI) with positron emission tomography (PET) using [ $^{15}\text{O}$ ]water is a standard tool in assessing MBF in patients with CAD but its feasibility in the assessment of myocardial viability is yet to be determined.

The most dramatic manifestation of IHD is myocardial infarction (MI), which usually is a result of a rupture of an atherosclerotic plaque and subsequent thrombosis within the artery lumen. MI is defined as acute myocyte necrosis following prolonged ischaemia (Thygesen et al., 2019). MI is followed by a three-phase healing process which includes inflammation, angiogenesis, fibroblast proliferation and eventually scar formation (Frangogiannis, 2006). Poor infarct healing can cause alterations in the LV involving both the infarcted and noninfarcted regions in a process defined as adverse LV remodelling, which can eventually lead to progressive LV dysfunction and development of chronic heart failure (HF). Despite developments in therapy, the prognosis of HF is generally poor as half of the patients with HF die within five years of the initial diagnosis (McMurray & Pfeffer, 2004). Angiogenesis, that is induced in the myocardial tissue after an ischaemic insult to preserve enough blood flow in the affected area, is an integral part of infarct healing. Integrin  $\alpha_v\beta_3$  is one of the most important integrins that regulate angiogenesis. Its expression is generally low in endothelial cells but elevated during angiogenesis. The detection of myocardial  $\alpha_v\beta_3$  integrin expression with PET using radiolabelled arginine-glycine-aspartic acid (RGD) peptides is a potential tool in monitoring LV remodelling after MI (Sherif et al., 2012).

In order to guide therapy and improve prognosis, identifying the patients with CAD and LV dysfunction that will most likely benefit from revascularisation or are at high risk for developing HF after MI is important.

In the studies of this thesis, MPI with [<sup>15</sup>O]water PET was studied for the assessment of myocardial viability after experimental MI. Also, the feasibility of a novel angiogenesis targeting PET tracer [<sup>68</sup>Ga]NODAGA-RGD was evaluated for the detection of integrin expression in a pig model of myocardial ischaemia. Finally, the uptake of [<sup>68</sup>Ga]NODAGA-RGD was studied in comparison to the amount of angiogenesis in an *in vitro* angiogenesis tissue model.

## 2 Review of the Literature

### 2.1 Ischaemic heart disease

#### 2.1.1 Coronary artery disease

The modern sedentary lifestyle in combination with high energy diet has led to high rate of ischaemic heart disease (IHD). The incidence of IHD has declined in the high-income countries during the last decades due to improved prevention and treatment but it, however, still remains the leading cause of death worldwide as the mortality is even increasing in low- and middle-income regions (Moran et al., 2014; Nowbar et al., 2019). Ischaemic heart disease, also called coronary artery disease (CAD), is caused by atherosclerosis in the epicardial coronary arteries, which eventually leads to narrowing of the artery lumen and myocardial ischaemia, i.e. decrease in the blood supply to myocardium. The main features of atherosclerosis are lipid accumulation into the intima with simultaneous inflammation. Atherosclerotic plaques start to develop already during childhood by formation of fatty streaks in the intima layer of the arteries (Stary et al., 1994). The disease progresses slowly over the decades and does not represent symptoms until at later stages of life. The fatty streaks evolve into atheromas, which might eventually grow to narrow the lumen of the artery leading to reduced blood flow and ischaemia, or rupture causing myocardial infarction (MI) (Gibson et al., 2018; Libby, 2002). CAD may present various symptoms depending on the severity of the stenosis. The first symptoms include shortness of breath and chest pain also called angina pectoris. These usually appear during exercise when the oxygen demand of the heart is increased and are absent at rest. In some cases, the first symptom of CAD might, however, be acute MI (Knuuti et al., 2020).

#### 2.1.2 Myocardial ischaemia and infarction

Reduced blood flow in the myocardium, most commonly due to atherosclerosis, results in an imbalance between the oxygen demand and supply and myocardium becomes ischaemic. Myocardium can shift between different substrates to produce energy in the form of adenosine triphosphate (ATP). In normal conditions ATP is

mainly produced by oxidising free fatty acids and to a lesser extent by metabolising carbohydrates and ketone bodies. However, for example during exercise or fasting, when lactate or ketone bodies become abundantly available myocardium utilises them in the energy production. In an ischaemic myocardium glycolysis is stimulated by hypoxia-inducible factor (HIF) 1 $\alpha$  and the energy is shifted towards glucose metabolism, which has better oxygen efficiency in the ATP production. (Kolwicz et al., 2013) The fate of the myocytes during ischaemia depends on the duration and degree of the ischaemia. Ischemia leads to impaired function of ion channels in the cell membrane and to myocyte oedema. Myocytes lose their contractile function, which may remain for days after the restoration of the blood flow. (McDiarmid et al., 2017; Stanley et al., 2005)

MI is pathologically defined as cardiomyocyte death caused by prolonged ischaemia (Thygesen et al., 2019). The first ultrastructural changes, such as diminished cellular glycogen, relaxed myofibrils, sarcolemmal disruption and mitochondrial abnormalities, occur already in 10-15 minutes after the onset of ischaemia (Thygesen et al., 2019). The injury caused by short period of ischaemia usually is reversible and the myocytes might survive if the blood flow is restored. Longer periods of ischaemia lead to irreversible injury and myocytes start to die by necrosis (Reimer et al., 1977). Ischaemia-induced necrosis is characterised by swelling of the cells, sarcolemmal disruption, mitochondrial calcification and inflammation (Majno & Joris, 1995; Reimer et al., 1977). The necrosis occurs first in the subendocardium and progresses transmurally (Reimer et al., 1977). It can, however, take several hours before complete cell death occurs depending on the amount of collateral flow, individual needs in myocardial oxygen consumption and recurring episodes of occlusion and reperfusion that lead to preconditioning of the heart (Thygesen et al., 2019). Diagnosis of MI is based on the rise and/or fall of circulating cardiac troponin (cTn) values, combined with clinical symptoms of ischaemia, changes in electrocardiography (ECG) or imaging evidence of coronary thrombus or ischaemia. (McDiarmid et al., 2017; Thygesen et al., 2019)

### 2.1.3 Healing after myocardial infarction

A repair process is initiated after the MI aiming to clear the infarct area from tissue debris and eventually replace the damaged myocardium with a scar. The infarct healing process is generally divided into three phases: the inflammatory phase, proliferative phase, and maturation phase. The rapid inflammatory response aims to clear the infarct area from cellular and extracellular matrix (ECM) debris during the first 4 days after the MI. The wound healing and neovascularisation begin as the proliferative phase takes place for the next couple of weeks. Finally, a scar is formed during the maturation phase, which takes approximately 2 months in large mammals.



The main events and cell types of infarct healing process are summarised in Figure 1 (Dobaczewski et al., 2010; Liehn et al., 2011).

### 2.1.3.1 Inflammatory phase

Injured cardiomyocytes activate the innate immune pathways and inflammatory response by releasing endogenous ligands called danger-associated molecular patterns (DAMPs). The released “danger signals” include high mobility group box 1 protein (HMGB1), heat shock proteins (HSPs), ATP, hyaluronan and fibronectin, among others (Andrassy et al., 2008; Arslan et al., 2011; Gupta et al., 2012). DAMPs activate the proinflammatory cascade mainly via toll-like receptors (TLRs) and interleukin-1 (IL-1) receptors in several cell types such as cardiomyocytes, endothelial cells, resident cardiac fibroblasts and mast cells, and newly recruited leukocytes and platelets. Downstream pathways, especially nuclear factor-kappa B (NF- $\kappa$ B), activated by TLRs and reactive oxygen species (ROS), enhance the expression of proinflammatory cytokines, for example tumor necrosis factor (TNF), IL-1 $\beta$ , IL-6 and IL-18, chemokines and cell adhesion molecules. (Arslan et al., 2011; Frangogiannis, 2014; Park et al., 2004)

Induced expression of chemokines attracts neutrophils, which are the first inflammatory cells to infiltrate the infarcted myocardium. Neutrophils participate in cleaning the area from dead tissue debris and increase the immune response. In addition to neutrophils, cytotoxic T-lymphocytes are early players in the infarction site. Monocytes are recruited to the infarction site in two phases. The early recruitment of monocytes shortly after the neutrophils consists of proinflammatory, phagocytic monocytes and M1 macrophages, whereas the monocytes and M2 macrophages arriving later have anti-inflammatory effects (Nahrendorf et al., 2007; Yan et al., 2013).

### 2.1.3.2 Proliferative phase

When the first days after the infarction are characterised by strong proinflammatory response, the proliferative phase begins with the suppression of the inflammation, which is essential for the reparative actions to begin. Neutrophils have a short life cycle and when at late stage and apoptotic, they start to release mediators, such as lipoxins, resolvins, annexin A1 and lactoferrin that inhibit neutrophil transmigration and promote apoptosis and phagocytic uptake of neutrophils by macrophages (Soehnlein & Lindbom, 2010). The neutrophils polarise macrophages towards anti-inflammatory and reparative M2 phenotype (Horckmans et al., 2017) that releases anti-inflammatory, pro-fibrotic and angiogenic mediators, such as IL-10, members of transforming growth factor (TGF)- $\beta$  family and vascular endothelial growth factor

(VEGF) (Soehnlein & Lindbom, 2010). Also, dendritic cells and regulatory T-lymphocytes infiltrate the infarcted myocardium and contribute to the suppression of inflammation. Some members of the chemokine family also play a role in suppressing inflammation by attracting anti-inflammatory subsets of monocytes and lymphocytes. (Prabhu & Frangogiannis, 2016)

As the inflammation resolves, reparative processes take place and healing of the infarct wound begins. Myofibroblasts cannot be found in healthy myocardium but they appear after injury and are the most abundant cell type in infarct scar replacing the dead cardiomyocytes and contributing to the formation of the scar (Turner & Porter, 2013). Myofibroblasts resemble fibroblasts and smooth muscle cells and they express several contractile proteins (such as  $\alpha$ -smooth muscle actin (SMA)), focal adhesion proteins (paxillin, tensin and  $\alpha_v\beta_3$  integrin), cell surface receptors (TGF- $\beta$  type II receptor and angiotensin AT1 receptor), structural ECM proteins (collagen I, collagen III and fibronectin), and matricellular proteins (periostin and osteopontin)(Turner & Porter, 2013). The contractile properties of myofibroblasts help in preventing infarct expansion (van den Borne et al., 2009). Myofibroblasts originate from several different cell types but the main source is most likely the resident fibroblasts that differentiate into myofibroblasts (Kanisicak et al., 2016; Yano et al., 2005). Endocardial epithelial cells can go through epithelial-mesenchymal transition and endothelial cells endothelial-mesenchymal transition to adopt a myofibroblast phenotype. Also, mesenchymal stem cells, fibrocytes, smooth muscle cells and pericytes are thought to be sources of myofibroblasts (Turner & Porter, 2013). The differentiation of the fibroblasts into myofibroblast is initiated by mechanical stress when the integrity of the ECM is lost due to the injury. First the fibroblasts become proto-fibroblasts, which further differentiate into myofibroblasts in response to biochemical signals, especially TGF- $\beta$  and fibronectin ED-A. Myofibroblasts can be found from infarct wounds years after the initial infarction. (van den Borne et al., 2009)

The restoration of the ECM begins with formation of provisional matrix that is composed mainly of fibrin and fibronectin. It is highly plastic and functions as a scaffold for the healing tissue. Several matricellular proteins bind to matrix proteins and cell receptors transducing signalling cascades. They do not, however give mechanical support. The structural matrix components are produced by myofibroblasts; first type III collagen and later type I collagen (Turner & Porter, 2013; van den Borne et al., 2009).

Angiogenesis is a process where new microvessels sprout from the pre-existing vessels. The formation of new vessels is needed to provide oxygen and nutrients to the healing tissue. In addition to the granulation tissue where the healing takes place, angiogenesis also occurs in the surrounding, viable myocardium (Cochain et al., 2013). Angiogenesis is initiated by activation of HIFs in cardiomyocytes, endothelial

cells, and inflammatory cells in the ischaemic area. HIFs induce the expression of angiogenic factors such as vascular VEGFs (Cochain et al., 2013). As a result, endothelial cells are activated, and changes in the basement membrane and endothelial cell junctions result in increased vascular permeability. The endothelial cells start to migrate guided by a specialised “tip cell”, which is followed by proliferating neighbouring endothelial cells that form the new sprout (Carmeliet & Jain, 2011). The sprouting of the new vessels begins from the infarct border zone (Zhao et al., 2010) and from the endocardium (Kobayashi et al., 2017), and then extends into the injured myocardium. The newly formed vessels are immature, leaky and disorganised before they enlarge and obtain a mural coat (Kobayashi et al., 2017). The maturation of the vessels is mediated by platelet-derived growth factor (PDGF). (Cochain et al., 2013).

Cells use adhesion molecules to interact with their surroundings and with other cells. One of the major groups of adhesion molecules is integrins which, during angiogenesis, mediate the adhesion between the tip cell and the ECM (Carmeliet & Jain, 2011). Integrins are heterodimeric transmembrane receptors, which consist of two glycoprotein subunits called  $\alpha$  and  $\beta$ . Several different heterodimer combinations of 18  $\alpha$  and 8  $\beta$  subunits form at least 24 integrin receptor variants in humans (Kim et al., 2011). Both  $\alpha$  and  $\beta$  subunits have an intracellular domain that interacts with the cytoskeleton and an extracellular domain that interacts with ECM proteins. Thus, integrins act as linkers over the cell membrane between the cell cytoskeleton and ECM or adjacent cells facilitating cell adhesion and movement and serving as mechanotransducers. (Manso et al., 2009) Their role is not, however, only limited to mechanical adhesive functions, since they also participate in signalling in bidirectional manner, either outside-in or inside-out (Takagi et al., 2002). In concert with for example G-protein-coupled or kinase receptors, integrins mediate various processes such as cell proliferation, differentiation, gene expression profile and apoptosis. (Hynes, 2002)

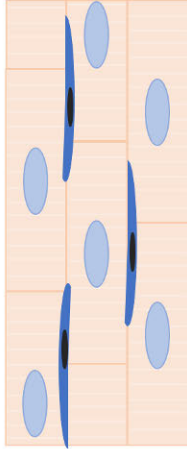
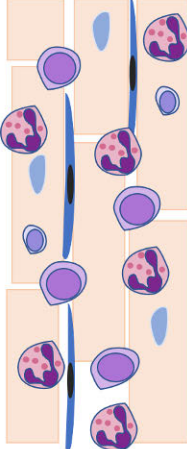
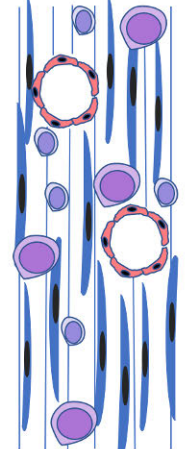
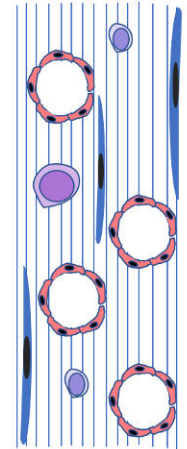

Depending on the subtype combination, integrins bind to several extracellular ligands, and reciprocally, one ligand can bind to several different integrins. Integrins can be divided into four distinct subfamilies based on the ligand recognition (Hynes, 2002). These include tripeptide sequence RGD binding integrins, laminin binding integrins, collagen binding integrins and leukocyte specific integrins (Hynes, 2002; Ruoslahti & Pierschbacher, 1987). RGD was first found to be an integrin binding motif in fibronectin and since that, it has been found in several other adhesive ECM proteins (Ruoslahti & Pierschbacher, 1987). RGD-based ligands bind to many integrin heterodimers, albeit with varying selectivity, and have been utilised in diagnosis and treatment of several disease states involving angiogenesis (Kapp et al., 2017). The ligand binding affinity of some integrins changes depending on the conformation of the integrin (Takagi et al., 2002). The trigger for the conformational

change from the inactive, bent conformation to the active, extended conformation comes from ligand binding or from the intracellular domains of the integrin receptor (Hynes, 2002).

Myocardium expresses several integrins such as  $\alpha_5\beta_1$ ,  $\alpha_v\beta_1$ ,  $\alpha_v\beta_3$ , and  $\alpha_v\beta_5$ , which regulate many processes during infarct healing and LV remodelling (Prabhu & Frangogiannis, 2016). They facilitate neutrophil adhesion to the endothelial cells on vessel wall before extravasation (Prabhu & Frangogiannis, 2016) and control macrophage activation (Antonov et al., 2011). Integrins activate latent TGF- $\beta$  contributing to myofibroblast differentiation and cardiac fibrosis (Murray et al., 2017; Sarrazy et al., 2014). Especially, the expression of  $\alpha_v\beta_3$  integrin is related to infarct healing process, since its expression is low in healthy myocardium but upregulated in endothelial cells during angiogenesis (Brooks et al., 1994). The expression of  $\alpha_v\beta_3$  integrin demonstrates subsequent functional recovery after MI in experimental and clinical studies (Jenkins et al., 2016; Sherif et al., 2012).

### 2.1.3.3 Maturation phase

During the maturation phase increased expression of crosslinking enzymes such as lysyl-oxidase promotes the crosslinking of the collagen. The reparative processes are run down and most of the reparative cells, such as myofibroblasts that have been active during the proliferative phase are inactivated or undergo apoptosis. By the end of the maturation phase the granulation tissue has matured into a dense collagen rich scar. (Prabhu & Frangogiannis, 2016)

Healthy myocardium	Inflammatory phase	Proliferative phase	Maturation phase
			
<b>Most prominent cell types</b>	<ul style="list-style-type: none"> <li>• Neutrophils</li> <li>• Proinflammatory monocytes and M1 macrophages</li> </ul>	<ul style="list-style-type: none"> <li>• Myofibroblasts</li> <li>• Apoptotic neutrophils</li> <li>• Anti-inflammatory monocytes and macrophages</li> <li>• Lymphocytes</li> </ul>	<ul style="list-style-type: none"> <li>• Anti-inflammatory monocytes and macrophages</li> <li>• Lymphocytes</li> <li>• Myofibroblasts</li> </ul>
<b>Healing events</b>	<ul style="list-style-type: none"> <li>• Myocyte death</li> <li>• Acute inflammation</li> <li>• Inflammatory cell recruitment</li> </ul>	<ul style="list-style-type: none"> <li>• Suppression of inflammation</li> <li>• Angiogenesis</li> <li>• Formation of provisional matrix</li> <li>• Collagen formation</li> </ul>	<ul style="list-style-type: none"> <li>• Apoptosis of reparative cells</li> <li>• Matrix cross-linking</li> <li>• Scar formation</li> </ul>
<b>Time scale</b>			

**Figure 1.** Events and cell types during different phases of infarct healing.

### 2.1.3.4 Adverse remodelling and heart failure

The optimal result after the infarct healing process is a strong scar that can maintain the size and shape of the LV. When the healing is not optimal, adverse remodelling takes place, leading to changes in LV size, shape and function, and changes in cellular and biochemical functions (Prabhu & Frangogiannis, 2016). One of the key features during LV remodelling is LV dilatation which is an attempt to compensate for the cell loss and following contractile dysfunction of the LV. Dilatation increases the myocyte stretch and leads to hypertrophy which, at first, helps to maintain stroke

volume, but eventually promotes further dilatation and dysfunction (Pfeffer & Braunwald, 1990). The LV remodelling is characterised by regression of the gene expression profile back to a fetal gene profile, especially regarding the genes related to metabolism and contractile proteins (Razeghi et al., 2001; Taegt Mayer et al., 2010). The initial purpose of all these changes is to compensate for the loss of the functioning myocardial tissue but instead they may lead to harmful effects, such as myocardial ischaemia and interstitial fibrosis, eventually resulting in the development of HF (Prabhu & Frangogiannis, 2016). The magnitude of adverse LV remodelling correlates with the extent of the myocardial injury (Chareonthaitawee et al., 1995; Wu et al., 2008), but also depends on other factors related to proper infarct healing (Westman et al., 2016). For example, impaired suppression of the inflammation and overactive fibrosis in the remote myocardium are predisposing factors to adverse remodelling. (Prabhu & Frangogiannis, 2016).

Inflammatory response after MI is needed for proper infarct healing but subsequent suppression of inflammation is equally important as too strong or prolonged inflammatory response may lead to persistent myocardial damage and inadequate scar formation. The higher expression of the proinflammatory cytokines IL-6, TNF, and IL-1 $\beta$  have been linked to LV remodelling in preclinical studies (Ono et al., 1998). Many cytokines, chemokines and other inflammatory mediators that promote remodelling, however, may also have cardioprotective effects during the healing process making therapeutic interventions complicated. (Prabhu & Frangogiannis, 2016)

Adequate density of myofibroblasts in the infarcted area is crucial for the formation of strong and flexible scar. Infarct expansion and LV dilatation with possible cardiac rupture occur when the amount of myofibroblasts in the infarcted region is too low. Too intense myofibroblast activation and collagen deposition especially in the remote myocardium, however, lead to myocardial stiffness and dysfunction. Several inflammatory cells, such as macrophages, mast cells and lymphocytes, activate myofibroblasts and fibrosis by secreting cytokines (for example TGF- $\beta$ 1 and IL-10) and matricellular proteins. (Frangogiannis, 2019; van den Borne et al., 2009). The activation of renin-angiotensin-aldosterone system (RAAS) contributes to the fibrosis during the adverse remodelling (Travers et al., 2016). Angiotensin II activates myofibroblasts directly and also by stimulating TGF- $\beta$ 1 production (Rosenkranz, 2004). TGF- $\beta$ 1 is the main contributor in fibrosis of the remote myocardium. It regulates myofibroblast differentiation and enhances the production of collagen, fibronectin and proteoglycans by cardiac fibroblasts (Rosenkranz, 2004). Both too high and too low myofibroblast density can lead to LV hypertrophy, reactive fibrosis, reduced cardiac output, arrhythmia and HF (Turner & Porter, 2013).

Sympathetic nervous system and RAAS become activated during the development of HF due to decrease in cardiac output. The activation of these neurohormonal systems and the changes they induce in other organs aim at keeping up the cardiovascular homeostatic balance but, in turn, contribute significantly to the progression of HF (Hartupee & Mann, 2016). HF is a condition where the heart is not able to pump blood efficiently enough for the metabolic needs of the body. The symptoms of HF are often non-specific, typically including shortness of breath and tiredness (Ponikowski et al., 2016). The diagnosis of HF relies on measurements of ECG, natriuretic peptides, and echocardiography. Other imaging modalities also may provide added value in uncertain cases (Ponikowski et al., 2016). Despite the developments in diagnosis and therapy, the prognosis of HF remains poor as more than half of the patients die within 5 years of the initial diagnosis. (Bleumink et al., 2004; Johansson et al., 2016)

#### 2.1.4 Myocardial viability

Dysfunctional ischaemic myocardium of patients with CAD often is a mixture of ischaemic but viable tissue and irreversibly injured scar tissue. In the presence of chronic or repetitive ischaemia, myocardium might go into the state of hibernation where the contractile function is missing and only the necessary metabolic activities are preserved in order to reduce the oxygen demand of the tissue and prevent myocyte necrosis (Rahimtoola, 1989; Ryan & Perera, 2018). The myocytes in hibernating myocardium are still alive i.e. viable and have the capability of regaining contractile function after revascularisation. Hibernation during myocardial ischaemia can be considered as a protective mechanism that keeps the myocytes alive. Hibernating myocardium increases the amount of glucose oxidative metabolism in order to produce enough ATP with less oxygen in comparison to oxidising fatty acids (Gewirtz & Dilsizian, 2017). Hibernating myocardium does not differ macroscopically from normal myocardium, but several histological, metabolic, and genetic changes have been found to take place. The cells switch from active contractile form to stable noncontractile form, which indicates cell dedifferentiation (Wijns et al., 1998). Microscopically, characteristics of dedifferentiation seen in the hibernating myocardium include loss of sarcomeres with aggregation of glycogen and mitochondria, loss of sarcoplasmic reticulum and redistribution of heterochromatin in the nucleus. (Wijns et al., 1998). The upregulation of genes related to cell survival, such as inhibitor of apoptosis (IAP), HSP70, H11 kinase (H11K), HIF-1 $\alpha$ , VEGF and glucose transporter 1 (GLUT1), along with upregulation of related proteins, contribute to the survival of the myocytes from prolonged hibernation. (Depre et al., 2004). Even though the hibernation is a protective mechanism during ischaemia it can, however, become irreversible over

time as adaptive mechanisms become insufficient. It has been shown that the cardiomyocyte degeneration and fibrosis are more severe and functional recovery after revascularisation less likely after longer period of ischaemia (Elsasser et al., 1997; Schwarz et al., 1998).

Viable myocardium also may be stunned, which refers to a state where viable myocardium exhibits contractile dysfunction as a result from an episode of transient ischaemia. Stunned myocardium does not represent extracellular changes. In comparison to hibernation, which might take 6-12 months to recover, the contractile function in stunned myocardium recovers in a couple of weeks after the restoration of blood flow (Patel et al., 2018).

## 2.2 Pig as an experimental model of chronic myocardial ischaemia

Pigs are one of the most used translational non-rodent animal models in preclinical studies. The heart and the coronary artery system of pigs are almost identical to those of humans, which make the pig an ideal animal model for translational cardiovascular research. The heart-to-body weight ratio is identical in humans and in the typical 30 kg pigs, which are commonly used in cardiovascular studies (Lelovas et al., 2014). The similar size of the heart and blood vessels enables the use of clinical scanners and equipment, and more reliable discrimination between the injured and ischaemic myocardial areas than in rodents. Pigs do not have existing collateral flow and thus, serve as a better cardiovascular large animal model than for example dogs, which have more extensive collateral network and are thus more difficult to induce MI (Hearse, 2000). The lack of collateral flow in pigs, however, makes them susceptible to transmural infarction after the occlusion (Swindle et al., 2012). Like humans, in normal conditions myocardium of pigs obtains most of its energy from free fatty acids, and in ischaemic conditions, by glucose metabolism (Lelovas et al., 2014). Also, infarct healing characteristics of pigs resemble humans more closely than many other species (Mehran et al., 1991). There are some limitations in the use of pigs. Growth rate of landrace pigs is high, which limits their use in long follow-up studies and might present some husbandry challenges. In regard of imaging studies, there might be problems with the limited size of the scanners. Pigs also tend to be vulnerable to ventricular arrhythmias and sudden cardiac death. (Lelovas et al., 2014; Swindle et al., 2012)

The most widely used methods to induce ischaemia in pigs usually are either surgical models most commonly using ameroid constrictor, or catheter-based percutaneous models (Hughes et al., 2003). The ameroid constrictor, composed of a hygroscopic inner ring, which is surrounded by a stainless-steel sheath, is placed around the coronary artery. The inner ring absorbs water and swells gradually



obstructing the lumen of the artery and resulting in reduction of the blood flow (Hughes et al., 2003). The placing of the ameroid constrictor requires thoracotomy, which is painful for the experimental animals and includes a risk for post-operative complications. Since pigs are susceptible to arrhythmias and sudden cardiac death after large MI, the model has been modified to include a distal ligation of the coronary artery before the placement of the ameroid constrictor, which improves the survival and produces larger infarcts (Teramoto et al., 2011). Surgical models also include fixed stenosis and hydraulic occluder-based models. The fixed degree of stenosis has an advantage of relatively similar degree of ischaemia in all pigs in comparison to ameroid constrictor model. Hydraulic occluder model also provides a fixed degree of stenosis, which can, however, be adjusted later. (Hughes et al., 2003)

Percutaneous catheter-based methods have also been developed. The chronic ischaemia can be produced by bottleneck (Rissanen et al., 2013) or hourglass (Von Degenfeld et al., 2003) shaped stents, or with copper (Horstick et al., 2009) or copper-coated (Wu et al., 2010) stents. The latter ones are based on neointimal hyperplasia induced occlusion after the stent implantation. In the bottleneck and hourglass stent models, the occlusion of the stent can be modulated with antiplatelet medication, which keeps the stent open for the desired period (Rissanen et al., 2013; Von Degenfeld et al., 2003). Endovascular methods are less invasive and easier on the animals and have lower risk for post-operative complications. They also are less laborious and faster to perform.

## 2.3 Myocardial perfusion imaging in ischaemic heart disease

Myocardial perfusion, i.e. the blood flow through the myocardium can be assessed non-invasively using nuclear imaging techniques single photon emission computed tomography (SPECT) and PET, and computed tomography (CT), magnetic resonance imaging (MRI) and echocardiography. Myocardial perfusion imaging (MPI) is useful in detecting CAD and estimating the hemodynamic significance of the stenosis. The size and location of ischaemic areas can be detected when the MPI is performed in both rest and stress conditions. Mild coronary stenosis resulting in reversible ischaemia is characterised by normal myocardial blood flow (MBF) at rest and reduced MBF during stress. In the case of severe stenosis and scar tissue, also rest perfusion may be reduced. (Cademartiri et al., 2017; Coelho-Filho et al., 2013; Tweet et al., 2015) Stress during the scanning can be induced by physical exercise or by pharmacological vasodilators, such as adenosine, regadenoson or dipyridamole (Saab & Hage, 2017).

### 2.3.1 Myocardial perfusion imaging with PET

MPI with PET is a standard tool in assessing perfusion defects in patients with CAD (Saraste et al., 2012). PET is a non-invasive molecular imaging technique based on the use of radiotracers at concentrations that do not affect biological processes. PET radiotracers consist of a molecular structure that is attached to a short half-life positron emitting radioisotope (Wadsak & Mitterhauser, 2010). When the radioisotope decays, it emits a positron that travels a short distance in the tissue before meeting an electron. Upon collision, positron and electron annihilate and produce two 511 keV gamma rays that travel in opposite directions and can be detected with the PET scanner's detectors that surround the subject circularly. The raw data from the scanner can then be reconstructed into an image using dedicated software (Phelps, 2000). An MPI PET tracer is retained in the myocardium proportional to blood flow and the myocardial blood flow can be measured at rest and under stress conditions to delineate the severity and extent of myocardial ischaemia. PET MPI tracers have relatively short physical half-lives and, therefore, the stress in PET studies needs to be induced by pharmacological agents. The unique feature of PET perfusion imaging is that blood flow can be quantified in absolute terms, i.e. in ml/g/min. This enables separate quantitation of MBF in each vascular territory and detection of three-vessel disease in which the MBF is reduced in all vascular territories. The quantification may, however, be limited to some extent by the perfusion dependent extraction fraction of some tracers (Figure 2). This results in non-linear tracer uptake and underestimation of higher flows, which can be corrected by mathematical models. The most commonly used PET perfusion tracers are partially extracted tracers [ $^{13}\text{NH}_3$ ] and [ $^{82}\text{Rb}$ ], and freely diffusible tracer [ $^{15}\text{O}$ ]water. (Driessen et al., 2017; Knuuti et al., 2009; Maddahi & Packard, 2014; Saraste et al., 2012)

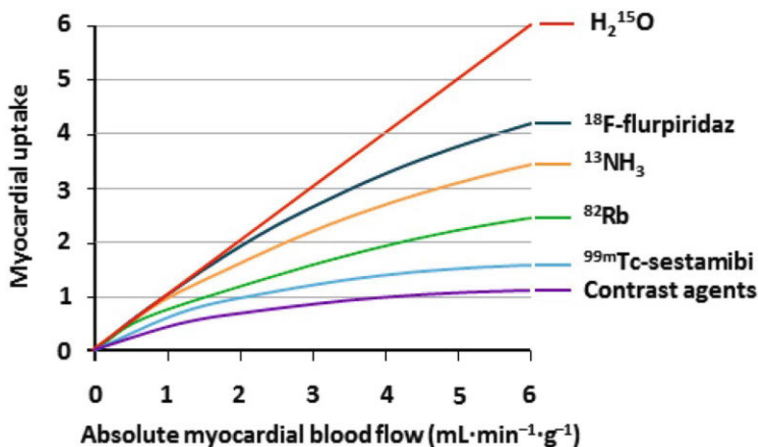


**Figure 2.** Relationship between absolute myocardial blood flow and tracer uptake (By Roel S. Driessen et al. (2017). "Myocardial perfusion imaging with PET". *International Journal of Cardiovascular Imaging* 33 (7): 1021–1031. DOI:10.1007/s10554-017-1084-4. PMC: 5489578., Wikimedia commons, CC BY 4.0) Accessed on 12.12.2019.

[<sup>13</sup>NH<sub>3</sub>] diffuses freely across cell membranes into the myocardial cells but is then converted to [<sup>13</sup>N]glutamine by *glutamine synthase*, and trapped inside the cells. It has a high extraction fraction that changes only little with higher flows. The physical half-life of [<sup>13</sup>NH<sub>3</sub>] is approximately 10 minutes making an on-site or a nearby cyclotron prerequisite. (Muzik et al., 1993; Schelbert et al., 1981)

Potassium analog [<sup>82</sup>Rb] is actively transported into the myocytes by Na/K ATP transporter. The physical half-life of [<sup>82</sup>Rb] is 76 seconds and it has a relatively low and flow-dependent extraction fraction, which needs to be corrected with modelling. It is, however, widely used due to its relatively easy availability with generator production (Saraste et al., 2012).

[<sup>15</sup>O]water is a metabolically and chemically inert, freely diffusible tracer with a flow-independent extraction fraction of practically 1, leading to a linear relationship between the myocardial uptake and MBF. Due to its ideal characteristics, [<sup>15</sup>O]water is considered the golden standard for quantification of myocardial perfusion and it detects myocardial ischemia with high diagnostic accuracy (Danad et al., 2014, 2017). A one-tissue compartment model is used in the [<sup>15</sup>O]water analysis. The quantification of segmental MBF with [<sup>15</sup>O]water can be done with good reproducibility using different scanners and softwares (Harms et al., 2014). Also, perfusable tissue fraction (PTF) and perfusable tissue index (PTI) can be obtained from the [<sup>15</sup>O]water scan. PTF is the amount of the tissue in the region of interest (ROI) that is capable of exchanging water rapidly, whereas PTI is the ratio of PTF and anatomical tissue fraction (ATF), which represents the mass of extravascular tissue inside the ROI. Thus, PTI is the fraction of the extravascular tissue that is

perfused by water. ATF is obtained by blood pool imaging with [<sup>15</sup>O]CO or by calculating parametric PTI images. (Harms et al., 2011; Iida et al., 1988, 1991) Due to the physical half-life of 123 seconds, [<sup>15</sup>O]water production is dependent on an on-site cyclotron.

A novel PET perfusion tracer [<sup>18</sup>F]flurpiridaz is currently undergoing phase III trial. It binds to mitochondrial complex-1 and is rapidly taken up by myocytes and retained in cardiomyocytes. [<sup>18</sup>F]flurpiridaz has a high extraction fraction and it has shown good results in clinical trials in relation to safety and in the detection of CAD. In comparison to other PET perfusion tracers, [<sup>18</sup>F]flurpiridaz has a physical half-life of 110 minutes, enabling transport and use also in imaging centres without an on-site cyclotron. In contrast to other PET perfusion tracers, [<sup>18</sup>F]flurpiridaz is useful with both pharmacological and exercise stress tests due to its longer half-life (Berman et al., 2013; Yalamanchili et al., 2007; Yu et al., 2007).

All of the above-mentioned PET MPI tracers have their advantages and disadvantages, and none meets all of the criteria for an optimal PET MPI tracer (Maddahi, 2012). The different characteristics of PET perfusion tracers are summarised in Table 1.

**Table 1** Characteristics of PET perfusion tracers.

	[ <sup>15</sup> O]water	[ <sup>13</sup> NH <sub>3</sub> ]	[ <sup>82</sup> Rb]	[ <sup>18</sup> F]flurpiridaz
Physical half-life	123 s	10 min	76 s	110 min
Production	Cyclotron	Cyclotron	Generator	Cyclotron
Kinetics	Freely diffusible, metabolically inert	Metabolically trapped in the myocardium	Metabolically trapped in the myocardium	Metabolically trapped in the myocardium
Max positron energy (keV)	1732	1198	3356	634
Positron range (mm)	4.14	2.53	8.6	1.03
Myocardial extraction fraction (%)	100	80	65	94

## 2.4 Imaging of myocardial viability

Since viable but dysfunctional myocardium can recover contractile function after revascularisation, the detection of viable myocardium is important in identifying the patients that benefit most from revascularisation. Viability imaging can be used to predict the probability of the myocardium to recover after revascularisation. If the patient does not have viable myocardium in the ischaemic area, the risks related to revascularisation procedures most likely outweigh the benefits. It has been shown that almost 40% of the patients who have ischaemic LV dysfunction exhibit improvement in LV function after revascularisation (Schinkel et al., 2004). Various non-invasive imaging techniques can be used to detect viable myocardium. The choice of the method should depend on the local expertise and availability, and on the additional information that is needed in addition to viability, since all the imaging modalities target different characteristics (Windecker et al., 2014). The assessment of viability alone is not meaningful but should be used in combination with the assessment of other variables for a comprehensive evaluation of patients. The main techniques for non-invasive assessment of myocardial viability are SPECT, PET, echocardiography, and cardiac magnetic resonance (CMR). The characteristics of different imaging techniques and their performance in the prediction of functional improvement are summarised in Table 2. (Bax & Delgado, 2015; Schinkel et al., 2007).

### 2.4.1 SPECT

Potassium analog  $^{201}\text{Tl}$ , and  $^{99\text{m}}\text{Tc}$  labelled compounds sestamibi and tetrofosmin are the most widely used SPECT tracers for the assessment of myocardial viability. The detection of viable tissue with  $^{201}\text{Tl}$  is based on perfusion and integrity of the cell membrane. After injection, the initial uptake of  $^{201}\text{Tl}$  reflects perfusion. The washout of  $^{201}\text{Tl}$  is quite fast and depends on MBF. Myocardial viability can be assessed from delayed images as  $^{201}\text{Tl}$  redistributes depending on the functional  $\text{Na}^+/\text{K}^+$  ATPase pump on myocyte cell membrane. (Henzlova et al., 2016; McDiarmid et al., 2017)

In comparison to  $^{201}\text{Tl}$ , tracers labelled with  $^{99\text{m}}\text{Tc}$  have better image quality because they emit higher energy photons. The assessment of myocardial viability with [ $^{99\text{m}}\text{Tc}$ ]tetrofosmin and [ $^{99\text{m}}\text{Tc}$ ]sestamibi depends on perfusion, cell membrane integrity and functional mitochondrial membranes. Sestamibi and tetrofosmin distribute passively across the membranes and bind to mitochondria where they are retained due to negative mitochondrial charge gradient, which is present only in viable myocytes (Caner & Beller, 1998; Henzlova et al., 2016).

## 2.4.2 PET

Glucose analog [ $^{18}\text{F}$ ]FDG is the most commonly used PET tracer and it is used to visualise glucose metabolism in cells. Like glucose, [ $^{18}\text{F}$ ]FDG is taken up by the cells via glucose transporters and then phosphorylated to FDG-6-phosphate. After phosphorylation, however, the tracer cannot proceed to the next steps of the glycolytic pathway and is trapped inside the myocytes. In normal conditions myocardium produces ATP mainly by oxidising free fatty acids but in an ischaemic myocardium the energy is obtained mainly by glucose metabolism and glucose transporters are upregulated. Since [ $^{18}\text{F}$ ]FDG is transported into the cells via glucose transporters, the upregulation of the transporters in ischaemic myocardium results in elevated uptake of [ $^{18}\text{F}$ ]FDG. (Bax et al. 2000) Viability imaging with [ $^{18}\text{F}$ ]FDG is combined with the assessment of perfusion. The detection of viable myocardium is based on a perfusion-metabolism mismatch, meaning elevated [ $^{18}\text{F}$ ]FDG uptake in combination with perfusion defect, while in scar tissue the [ $^{18}\text{F}$ ]FDG uptake and perfusion are both decreased. (Tillisch et al., 1986)

Also, PTF and PTI derived from the measurement of MBF by [ $^{15}\text{O}$ ]water PET, have been studied to evaluate viability. Since scar tissue cannot exchange water rapidly, PTF and PTI both are reduced in the absence of viable tissue (Iida et al., 2000; Knaapen et al., 2003, 2006). They both have been shown to detect viability and predict recovery of contractile function after revascularisation in patients with acute (Timmer et al., 2017; Yamamoto et al., 1992) or old MI (Bondarenko et al., 2011; de Silva et al., 1992; Iida et al., 2012; Itoh et al., 2002).

The oxidative metabolism and perfusion can be imaged with  $^{11}\text{C}$ -labelled acetate. Acetate is quickly transported into myocytes and converted into acetyl-CoA. The build-up phase of the radioactivity after the injection of [ $^{11}\text{C}$ ]acetate is related to perfusion. Acetyl-CoA is further oxidised to  $\text{CO}_2$  in the tricarboxylic acid cycle in mitochondria. The clearance rate of [ $^{11}\text{C}$ ] $\text{CO}_2$  from the tissue represents the oxygen consumption and is higher in the viable than in the non-viable myocardium. (Grassi et al., 2012; Klein et al., 2001)

## 2.4.3 Echocardiography

The use of echocardiography in the viability assessment is mainly based on the detection of contractile reserve during dobutamine stress. Dobutamine infusion is started with a low dose and increased gradually. Viable but ischaemic myocardium exhibits a biphasic response to stepwise infusion of dobutamine. The contractile dysfunction improves during low dose infusion if the tissue is viable but is then followed by worsening as the dose is increased (Senior & Lahiri, 1995). The end diastolic wall thinning (EDWT) can be assessed from resting echocardiography images. The LV wall thickness may be reduced in the areas of transmural infarction,

and a thickness of  $\leq 6$  mm seems to exclude functional recovery after revascularisation (Cwajg et al., 2000).

#### 2.4.4 Cardiac magnetic resonance imaging

Several CMR techniques have been used for the assessment of myocardial viability. Like with dobutamine stress echocardiography, contractile reserve can be detected with CMR during dobutamine infusion. CMR also allows detection of the transmural extent of the scar using gadolinium-based contrast agents, which stay in the interstitial space in the tissue. Scar tissue has more interstitial space and thus enhancement of gadolinium can be seen in the scar area. Also, EDWT associated with transmural scar can be detected with CMR. (Kaandorp et al., 2005)

**Table 2** Characteristics of different techniques for assessment of myocardial viability. Sensitivities and specificities from Schinkel et al. 2007.

Technique	Imaging finding	Prediction of improvement in regional function	
		Sensitivity (%)	Specificity (%)
SPECT			
• [ <sup>201</sup> Th]	Perfusion, cell membrane integrity	87	54
• [ <sup>99m</sup> Tc]	Perfusion, cell membrane integrity, intact mitochondria	83	65
PET			
• [ <sup>18</sup> F]FDG	Glucose metabolism	92	63
• [ <sup>15</sup> O]water	PTF, PTI		
• [ <sup>11</sup> C]acetate	Oxidative metabolism, perfusion		
Dobutamine stress echocardiography	Contractile reserve	80	78
Cardiac magnetic resonance imaging			
• Resting	End diastolic wall thickness	95	41
• Dobutamine infusion	Contractile reserve	74	82
• Gadolinium based contrast agents	Scar tissue	84	63

## 2.5 PET imaging of myocardial injury and angiogenesis

PET imaging of different molecular processes that are related to infarct healing and LV remodelling provide potential tools in detecting the patients who are at higher risk for developing HF after MI. Additionally, they may provide help in planning of the treatments. PET tracers for different infarct healing characteristics are summarised in Table 3.

### 2.5.1 Inflammation

Inflammatory response after MI is complex and closely linked to the reparative actions. Since many characteristics of inflammatory response have both beneficial and detrimental roles during the infarct healing depending on their temporal occurrence, selective detection of injurious characteristics is needed to guide therapeutic approaches aiming to modulate inflammatory response.

[<sup>18</sup>F]FDG is the mostly used PET tracer in imaging inflammation in various diseases. Myocardium shows increased [<sup>18</sup>F]FDG uptake after MI. The uptake seems to be localised on monocytes and macrophages by a preclinical study (Lee et al., 2012), and correlate inversely with functional outcome in patients 6 months after the MI (Rischpler et al., 2016). Ischaemic myocardium obtains energy from glucose metabolism and remaining viable cardiomyocytes can show high [<sup>18</sup>F]FDG uptake. To prevent the unspecific uptake patients can be subjected to high fat diet, fasting, and heparin injection prior to the scan. (Rischpler et al., 2016)

[<sup>11</sup>C]methionine uptake reflects protein synthesis and amino acid transport but it also accumulates into sites of inflammation and tissue repair. [<sup>11</sup>C]methionine accumulates in the infarcted area at early phase of infarct healing in experimental animals and humans. The accumulation seems to be localised in proinflammatory M1 macrophages. (Morooka et al., 2009; Thackeray et al., 2016).

Another possible target for PET imaging of inflammation is the chemokine receptor CXCR4, which is involved in recruitment and homing of stem cells and leukocytes into the infarcted region. CXCR4 binding PET tracer [<sup>68</sup>Ga]pentixafor has been studied after MI in preclinical studies and in patients. In mice the infarcted area shows higher tracer uptake, which corresponds with leukocytes (Thackeray et al., 2015). Patients have shown high interindividual variability in the [<sup>68</sup>Ga]pentixafor uptake (Lapa et al., 2015) but it, however, has been shown to correlate with smaller scar volume after healing (Reiter et al., 2018).

There is some limited evidence of imaging post-infarction inflammation with mitochondrial translocator protein (TSPO) targeted tracers. The uptake of [<sup>18</sup>F]GE180 has been shown to detect inflammation early after infarction and predict



later occurrence of LV remodelling. Later uptake is not related to inflammatory cells, suggesting myocyte mitochondrial impairment (Thackeray et al., 2018).

### 2.5.2 Angiogenesis

The expression of  $\alpha_v\beta_3$  integrin is normally low in endothelial cells but highly upregulated during angiogenesis, making it a potential target for imaging postinfarction angiogenesis (Brooks et al., 1994). In addition to mediating angiogenesis,  $\alpha_v\beta_3$  integrin also plays a role in the regulation of other characteristics of the infarct healing process, such as macrophage inflammatory responses and myofibroblast differentiation (Antonov et al., 2011; Sarrazy et al., 2014). Tripeptide sequence RGD is an integrin binding motif that can be radiolabelled and used in the detection of  $\alpha_v\beta_3$  integrin expression after MI (Gao et al., 2012; Higuchi et al., 2008; Kiugel et al., 2014; Laitinen et al., 2013; Menichetti et al., 2013; Sherif et al., 2012). The RGD tracer uptake is visible already 3 days after the infarction, peaks between 1 and 4 weeks, and stays in the detectable level even for 6 months after the MI (Higuchi et al., 2008; Kiugel et al., 2014; Meoli et al., 2004). The elevated uptake of RGD based tracers has been shown to be associated with the absence of significant LV remodelling after experimental MI (Sherif et al., 2012), and probability of functional recovery in patients with acute MI (Jenkins et al., 2016). Tracers containing RGD motif also provide a potential tool for monitoring the effects of angiogenesis inducing therapies (Cai et al., 2016; Johnson et al., 2008). The use of RGD peptides has been evaluated not only for imaging angiogenesis, but also other characteristics of LV remodelling such as myofibroblasts (van den Borne et al., 2008).

While  $\alpha_v\beta_3$  integrin targeted RGD tracers are the most studied angiogenesis imaging probes, also some other angiogenesis related targets, for example  $\alpha_5\beta_1$  integrin, CD13, CD105 and VEGF, have been preclinically evaluated (Mandic et al., 2016; Orbay et al., 2013).

### 2.5.3 Fibrosis

CMR is the most used method for detecting myocardial fibrosis but PET enables specific assessment of the molecular processes related to the formation of fibrosis. Activated RAA system is an important mediator in the formation of fibrosis contributing to myofibroblast differentiation through activation of TGF- $\beta$ , thus providing a potential target for the assessment fibrosis. An angiotensin-converting enzyme (ACE) inhibitor [18F]fluorobenzoyl-lisinopril has been tested in human explanted hearts where it binds specifically to ACE in the areas adjacent to collagen replacement (Dilsizian et al., 2007). [11C]KR31173 is a tracer that binds to

angiotensin II subtype 1 receptors (AT1R). It has been shown to accumulate in the ischaemic and remote myocardium after MI in pigs. The first clinical study also showed accumulation in the healthy heart, although at lower level than pigs (Fukushima et al., 2013). ACE is an excreted enzyme, which makes it less suitable as an imaging target than receptors such as AT1R or TGF- $\beta$  (van den Borne et al., 2009). Some TGF- $\beta$  targeted tracers already exist, but they have not been assessed in MI (Rotteveel et al., 2019).

**Table 3** Established and experimental PET tracers for imaging different characteristics of infarct healing process

Characteristic	Tracer	Target
Inflammation	[ <sup>18</sup> F]FDG	Monocytes and macrophages
	[ <sup>11</sup> C]methionine	Proinflammatory M1 macrophages
	[ <sup>68</sup> Ga]pentixafor	CXCR4 chemokine receptor
	[ <sup>18</sup> F]GE180	Mitochondrial translocator protein (TSPO)
Angiogenesis	RGD	$\alpha_v\beta_3$ integrin
		$\alpha_5\beta_1$ integrin
		CD13
		CD105
		VEGF
Fibrosis	[ <sup>18</sup> F]fluorobenzoyl-lisinopril	ACE
	[ <sup>11</sup> C]KR31173	AT1R
		TGF- $\beta$

## 3 Aims

The purpose of this study was to develop new translational technology for non-invasive imaging of myocardial ischaemic injury based on quantification of perfusion and molecular targeting of angiogenesis in large animal models that closely resemble human ischaemic heart disease. Furthermore, we aimed at validating molecular targeting of angiogenesis in an angiogenesis tissue model. The individual aims of the three studies in this thesis were:

1. To evaluate resting MBF, PTF, and PTI measured with [ $^{15}\text{O}$ ]water PET for the detection of infarcted and viable myocardium in comparison to histology in experimental models of chronic myocardial infarction.
2. To study the feasibility of non-invasive imaging of integrin expression with the use of [ $^{68}\text{Ga}$ ]NODAGA-RGD PET after reversible or irreversible chronic ischaemic myocardial injury in the pig heart.
3. To quantitate the [ $^{68}\text{Ga}$ ]NODAGA-RGD uptake in comparison to the amount of angiogenesis in human cell-based 3D *in vitro* model of angiogenesis.

## 4 Materials and Methods

### 4.1 Animal models (I, II)

Finnish landrace pigs were used in the animal experiments. All animal experiments were approved by the Lab-Animal Care & Use Committee of the State Provincial Office of Southern Finland and carried out in compliance with the EU legislation relating to the conduct of animal experimentation.

#### 4.1.1 Study outline (I, II)

In subproject I, 20 pigs with a TTC confirmed MI and PET myocardial perfusion imaging performed were retrospectively evaluated. 4 pigs were implanted with a bottleneck stent in the proximal LAD, and 16 pigs underwent a 2-step occlusion of LAD. Pigs were imaged with [<sup>15</sup>O]water at rest 2 weeks or 3 months after the stenting or surgical operation, respectively. Then, hearts were excised and stained with TTC.

In subproject II, 11 pigs were implanted with a bottleneck stent in the proximal LAD. 2 weeks after the stent implantation, pigs were imaged with [<sup>15</sup>O]water at rest and during adenosine-induced stress, and with [<sup>68</sup>Ga]NODAGA-RGD. Three pigs with no perfusion defect during stress were excluded from further analyses. After imaging, the hearts were excised for immunohistochemical stainings and *ex vivo* analyses.

#### 4.1.2 Anaesthesia and hemodynamic monitoring (I, II)

The animals were anaesthetised with intramuscular (i.m) injection of midazolam 1 mg/kg (Midazolam Hameln, Hameln Pharmaceuticals GmbH, Hameln, Germany) and xylazine 4 mg/kg (Rompun vet, Bayer Animal Health GmbH, Leverkusen, Germany). Anaesthesia was maintained with intravenous (i.v.) infusion of propofol 10–50 mg/kg/h (Propofol-Lipuro, B. Braun Melsungen AG, Melsungen, Germany) combined with fentanyl 4–8 µg/kg/h (Fentanyl-Hameln, Hameln Pharmaceuticals GmbH, Hameln, Germany) via cannulated ear vein under mechanical ventilation with tidal volume of 8-10 ml/kg and frequency of 14-18 breaths per minute (Dräger Oxylog 3000, Drägerwerk AG, Lübeck, Germany). Diastolic, systolic, and mean

arterial pressure and heart rate were recorded via cannulated femoral artery using a pressure transducer (TruWave, Edwards Lifesciences, Irvine, CA, USA).

#### 4.1.3 Bottleneck stent model for myocardial ischaemia (I, II)

The implantation of the bottleneck stent has been previously described (Rissanen et al., 2013). First, an introducer sheath (6F, Cordis, Bridgewater, NJ, USA) was placed percutaneously in the femoral artery. Pigs were catheterized with a GE Innova 3100<sup>IQ</sup> 3D angiography device (GE Healthcare, Waukesha, WI, USA). A sterilized polytetrafluoroethylene tube (diameter 5/64 in.; Fluorplast, Petalax, Finland) with a bottleneck diameter of 0.9 mm on the other end of the tube on a Coroflex Blue Ultra (B. Braun Medical; profile 0.8 mm) bare metal stent was placed into the proximal left anterior descending (LAD) coronary artery. A Femostop device (St. Jude Medical, St. Paul, MN, USA) was used to secure hemostasis after the removal of the sheath.

Amiodarone 200 mg/day per orally (p.o.) (Cordarone, Sanofi, Paris, France) and bisoprolol 2.5 mg/day p.o. (Bisoproact, Actavis Group, Hafnarfjordur, Island) were administered starting 1 week before the stenting until the end of the study to prevent arrhythmias. 750 mg i.v. bolus of Cefuroxime (Zinacef, GlaxoSmithKline, Brentford, UK), 100 mg i.v. bolus of lidocaine (Lidocain, Orion Corporation, Espoo, Finland) and 2.5 ml i.v. bolus of magnesium sulphate (246 mg/ml, Addex-magnesiumsulfaatti, Fresenius Kabi AB, Uppsala, Sweden) were administered immediately before the catheterization. Acetylsalicylic acid 300 mg p.o. (Primaspan, Orion Corporation, Espoo, Finland) was given 1 day before stenting and daily dose of 100 mg p.o. was continued throughout the study. Also clopidogrel 300 mg p.o. (Plavix, Sanofi, Paris, France) was given 1 day before stenting and continued throughout the study with a dose of 75 mg/day p.o. Enoxaparin 30 mg i.v. (Sanofi, Paris, France) was administered after the insertion of an introducer sheath in the femoral artery, and another 30 mg was given subcutaneously (s.c.) after removing the sheath and securing hemostasis. Daily dose of enoxaparin (30 mg/day s.c.) was continued throughout the study.

#### 4.1.4 Ameroid model (I)

A two-step ligation of LAD was performed surgically. Short left anterior thoracotomy was performed and pericardium was opened. Complete ligation of the distal LAD was first performed using a 5-0 monofilament polypropylene suture (Prolene, Ethicon, Norderstedt, Germany). Approximately 15 minutes after the ligation of distal LAD, an ameroid constrictor (2.50 or 2.75 mm, model MRI-2.50-

TI and MRI-2.75-TI; Research Instruments SW, Escondido, CA, USA) was placed around the proximal LAD.

Pigs were administered 30 mg/kg i.v. bolus of cefuroxime (Cefuroxime, Orion Pharma, Espoo, Finland) before the operation. The thoracotomy wound was anaesthetized with 25 mg i.m. injection of bupivacain (Bicain, Orion Pharma, Espoo, Finland) at the end of the operation. Fentanyl 2-4 µg/kg/hour (Matrifen transdermal patch, Takeda Pharma A/S, Roskilde, Denmark) was administered postoperatively for 3-7 days.

Amiodarone (Cordarone, Sanofi-Synthelabo Ltd., Newcastle upon Tyne, UK) was administered 8 mg/kg perorally (p.o.) daily starting 1 week before and lasting for 2 weeks after the surgery. Amiodarone 6 mg/kg i.v., metoprolol 2 mg/kg i.v. (Seloken, Genexi, Fontenay sous Bois, France) and magnesium sulfate (MgSO<sub>4</sub>) 25 mg/kg i.v. (Addex-magnesiumsulfaatti, Fresenius Kabi AB, Uppsala, Sweden) were intraoperatively administered. Administration of Clopidogrel 3 mg/kg p.o. (Plavix, Sanofi Winthrop Industrie S.A., Ambare's et Lagrave, France) was started 1 day before and continuing for 2 weeks after the surgery to prevent premature thrombosis of the LAD.

## 4.2 *In vivo* PET studies

### 4.2.1 Imaging myocardial perfusion with [<sup>15</sup>O]water PET (I, II)

In study I, the myocardial perfusion PET study with [<sup>15</sup>O]water at rest was performed 2 weeks after the stent implantation or 3 months after the surgical operation, and in study II, the myocardial perfusion studies at rest and under pharmacological stress were performed 2 weeks after the stent implantation with a Discovery 690 hybrid PET/CT scanner (GE Medical Systems, Milwaukee, WI, USA). [<sup>15</sup>O]water was injected as an i.v. bolus over 15 s at an infusion rate of 10 ml/min via the ear vein. A 4 min 40 s dynamic scanning was performed with time frames 14 × 5 s, 3 × 10 s, 3 × 20 s and 4 × 30 s. An adenosine infusion at the rate of 200–500 µg/kg/min combined with phenylephrine 5 µg/kg/min was started 120 s before the [<sup>15</sup>O]water injection and continued until the end of the scan. The acquired [<sup>15</sup>O]water PET data were corrected for scatter, random counts and dead time. An iterative VUE Point algorithm using 2 iterations and 24 subsets was used for reconstruction. The whole transaxial field of view (70 cm) was reconstructed in 128 × 128 matrix yielding pixel size of 5.47 mm × 5.47 mm. The device produces 47 axial planes with a slice thickness of 3.27 mm.

## 4.2.2 Imaging integrin expression with [<sup>68</sup>Ga]NODAGA-RGD (II)

[<sup>68</sup>Ga]NODAGA-RGD PET was performed with an ECAT EXACT HR+ scanner (Siemens-CTI, Knoxville, TN, USA) right after the [<sup>15</sup>O]water studies. After a 10 min transmission scan,  $310 \pm 43$  MBq of [<sup>68</sup>Ga]NODAGA-RGD was injected via the ear vein. The 62 min dynamic scanning (acquisition time frames:  $18 \times 10$  s,  $4 \times 30$  s,  $2 \times 120$  s,  $1 \times 180$  s,  $4 \times 300$  s and  $3 \times 600$  s) started at the same time with the tracer injection. The acquired [<sup>68</sup>Ga]NODAGA-RGD PET data were corrected for scatter, random counts, and dead time and iteratively reconstructed with ordered-subsets expectation maximization (OSEM) algorithm using 2 iterations and 32 subsets. The whole transaxial field of view (70 cm) was reconstructed in  $256 \times 256$  matrix yielding to pixel size of  $2.57 \text{ mm} \times 2.57 \text{ mm}$ . The device produces 63 axial planes with a slice thickness of 2.43 mm.

## 4.2.3 PET image analyses (I, II)

Carimas 2.9 software with Heart and PolarRoi plug-in tools (Turku PET Centre, Turku, Finland) was used for the analyses of the PET images. In [<sup>15</sup>O]water images, the long axis was manually defined and the myocardial contours were semi-automatically defined and the volume of interest (VOI) covering the whole LV myocardium was applied. The PTF and absolute segmental LV MBF were quantified from [<sup>15</sup>O]water data as ml/min/g using a single-compartment model as described earlier (Iida et al., 1991, 1992), and displayed as a standard 17 segment polar map. (I, II)

To obtain the relative MBF values in study I, the polar maps of [<sup>15</sup>O]water at rest were normalised to mean value of four posterolateral segments (segments 4, 5, 10, and 11), which were outside the ischaemic area. Posterolateral segments that were infarcted according to 2,3,5-triphenyltetrazolium chloride (TTC) staining, were excluded from the mean value. To study the reproducibility of the measurements, the analyses were performed twice by the same observer, and within-subject coefficients of variations were calculated by using root-mean-square approach. Coefficients of variations for repeated measurements of absolute MBF, relative MBF, and PTF measurements were 6% in the remote non-infarcted segments. In segments with infarct volume fraction  $\geq 75\%$ , coefficients of variations were 19%, 18%, and 10%, respectively.

In transmurally infarcted myocardium the thickness of the LV wall may be reduced. The effect of ROI thickness on absolute MBF, relative MBF, and PTF was evaluated by manually increasing or reducing ROI thickness from default. In further analyses, ROI thickness was manually reduced to completely fit inside the myocardium. MBF and PTF in viable and non-viable myocardium of the pigs that

had transmural infarction were further compared by analysing their circumferential profiles in 48 sectors in midventricular level. Values were compared between the transmurally infarcted non-viable area (average of three adjacent sectors) and remote viable areas (average of six sectors). For PTI measurements, a subset of pigs were further analysed with aQuant software (MedTrace Pharma A/S, Denmark) as described earlier (Harms et al., 2011).

In study II, for quantification of  $[^{68}\text{Ga}]\text{NODAGA-RGD}$  uptake in the myocardium, the  $[^{15}\text{O}]\text{water}$  images and the  $[^{68}\text{Ga}]\text{NODAGA-RGD}$  images were co-registered using the high blood pool activity of the  $[^{68}\text{Ga}]\text{NODAGA-RGD}$  as a landmark (Figure 3). The myocardial contours from the  $[^{15}\text{O}]\text{water}$  images were copied to the co-registered  $[^{68}\text{Ga}]\text{NODAGA-RGD}$  data. Then, the polar maps of  $[^{68}\text{Ga}]\text{NODAGA-RGD}$  uptake expressed as standardized uptake value (SUV) (time frame 52–62 min after injection) in the LV myocardium were generated. The ROI defining the ischaemic area (region with myocardial blood flow less than 80% of maximum during adenosine-induced stress as previously described (Kajander et al., 2011)) was copied from the  $[^{15}\text{O}]\text{water}$  polar maps to measure  $[^{68}\text{Ga}]\text{NODAGA-RGD}$  uptake in this region. The septum was excluded from the measurements to prevent spill over from the blood in the right ventricle. The mean and maximum SUVs were determined from the ischaemic area. In order to measure the SUVs, ROI was modified to include only the mid-myocardium in order to avoid spill-over from blood. The maximum SUV within the ROI was determined from area showing visually the highest uptake. One segment in the posterolateral wall (segment 11) that was always outside the ischaemic area was used to measure  $[^{68}\text{Ga}]\text{NODAGA-RGD}$  uptake in the remote myocardium. The ischaemic-to-remote SUV ratio was calculated in the ischaemic area and remote myocardium.

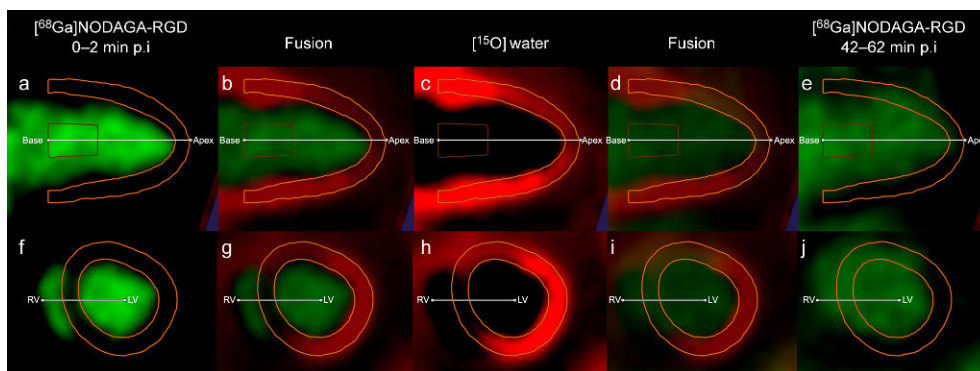


**Figure 3.** Co-registration of  $[^{68}\text{Ga}]\text{NODAGA-RGD}$  and  $[^{15}\text{O}]\text{water}$  PET images. Panels a and f demonstrate  $[^{68}\text{Ga}]\text{NODAGA-RGD}$  images during the first 2 min after injection of the tracer, and panels e and j during the last 20 min of the imaging session. Panels c and h demonstrate  $[^{15}\text{O}]\text{water}$  PET images, which are fused with  $[^{68}\text{Ga}]\text{NODAGA-RGD}$  images at different time points in images b and g, and d and i. From original publication II.



## 4.3 Tissue analyses

The pigs were sacrificed after the PET scanning with an i.v. injection of potassium chloride (B. Braun Medical Oy, Helsinki, Finland). The heart was excised, and LV was cut into 4 short axis slices from base to apex.

### 4.3.1 TTC (I, II)

To visualize the non-viable ischaemic area, LV slices were incubated for 15 min in 1% TTC (Sigma-Aldrich, Saint Louis, MO, USA), diluted in phosphate-buffered saline (PBS) (pH 7.4) at 37 °C and photographed from both sides. TTC staining differentiated between metabolically active viable and metabolically inactive non-viable tissue. TTC stains viable tissue deep red and leaves the non-viable tissue pale, almost white.

In study I, the infarct size was estimated from the TTC photographs visually. The heart was divided into segments using a standard 17 segments division. The volume fraction of the infarct in each segment was categorized as follows: 0: no infarct; 1: infarct size < 25%; 2: 25% – < 50%; 3: 50% – < 75%, and 4:  $\geq$  75% of the size of the segment. The apical segment 17 was excluded from the analyses.

In study II, transmural samples were collected according to the TTC staining from the non-viable area, immediately adjacent viable area, and from the remote area in the posterior LV wall.

### 4.3.2 *Ex vivo* autoradiography (II)

Tissue samples from the non-viable area, immediately adjacent viable area, and from the remote area were frozen in isopentane and cut into 40  $\mu$ m sections for autoradiography. Sections were immediately exposed on a phosphor imaging plate (BAS-TR2025, Fuji Photo Film Co. Ltd., Tokyo, Japan) for two hours. After exposure the plates were scanned with Fluorescent Image Analyzer (Fujifilm FLA-5100, Fuji Photo Film Co. Ltd., Tokyo, Japan). The distribution of [ $^{68}$ Ga]NODAGARGD was measured by drawing ROIs covering remote myocardium, and viable or injured ischaemic myocardium using TINA<sup>TM</sup> 2.10f software (Raytest Isotopenmessgeräte GmbH., Straubenhardt, Germany). Results were expressed as photostimulated luminescence per square millimetre (PSL/mm<sup>2</sup>) and normalized for the injected radioactivity dose, animal weight and the radioactivity decay.

### 4.3.3 *Ex vivo* biodistribution (II)

Myocardial samples from the non-viable area, immediately adjacent viable area, and from the remote area in the posterior LV wall were weighed and measured for

radioactivity using the gamma counter (Wizard 3<sup>™</sup>; PerkinElmer/Wallac, Turku, Finland). The radioactivity concentration was expressed as standardized uptake values ( $SUV = ([\text{tissue radioactivity}/\text{tissue weight}]/[\text{total given radioactivity}/\text{animal body weight}])$ ).

#### 4.3.4 Histology and immunohistochemistry (II)

##### 4.3.4.1 General histology

Frozen sections of 7  $\mu\text{m}$  of myocardial samples from the non-viable area, immediately adjacent viable area, and from the remote area in the posterior LV wall were stained with hematoxylin and eosin to visualize general histology. Masson's trichrome staining was used to distinguish cardiomyocytes and collagenous scar.

##### 4.3.4.2 Immunohistochemical stainings of CD31, $\alpha_v\beta_3$ integrin and $\alpha$ -SMA

Samples from the non-viable area, immediately adjacent viable area, and from the remote area were stained with antibodies against  $\alpha_v\beta_3$  integrin (dilution 1:200, Millipore, Temecula, CA, USA), CD31 to visualize endothelial cells and angiogenesis (dilution 1:250, Thermo Scientific, Cheshire, UK) and  $\alpha$ SMA to visualize myofibroblast differentiation (dilution 1:30 000, Sigma-Aldrich, St. Louis, MO, USA).

### 4.4 *In vitro* experiments

#### 4.4.1 Plasma protein binding (II)

Binding of [ $^{68}\text{Ga}$ ]NODAGA-RGD to human, pig and rat plasma proteins was measured using an *in vitro* assay as described previously (Tarkia et al., 2012).

#### 4.4.2 Angiogenesis tissue model (III)

Human cell-based 3D-model of angiogenesis was obtained from FICAM, Finnish Centre of Alternative Methods. Human adipose stromal cells (hASC) and human umbilical vein endothelial cells (HUVEC) were co-cultured on plastic coverslips placed in 24-well plate for receptor binding studies, or on chamber microscope slides for autoradiography studies. The tubule network formation was stimulated with growth factors VEGF and FGF- $\beta$ . Four different growth factor concentrations were used to obtain gradient in tubule network density. The maximal inductive

concentrations were 10 ng/ml VEGF and 1 ng/ml FGF- $\beta$ , which were reduced 25%, 50%, and 75%. Co-culture of hASC and HUVEC cells without induction of tubule network using growth factors was used as a control.

The use of the human fat tissue/umbilical cords was permitted by Local Ethics Committee in accordance with International Conference on Harmonisation (ICH) GCP guidelines (CPMP/ICH/135/95) and the World Medical Association Declaration of Helsinki (1964) and subsequent amendments.

#### 4.4.3 *In vitro* receptor binding (III)

[<sup>68</sup>Ga]NODAGA-RGD was added on 24-well plates and incubated for 90 minutes at 37°C. After dip-washing with PBS, the cover slips containing the vessels were removed from the wells and measured for radioactivity using gamma counter (Wizard 3<sup>™</sup>; PerkinElmer/Wallac, Turku, Finland).

#### 4.4.4 *In vitro* autoradiography (III)

For the autoradiography, [<sup>68</sup>Ga]NODAGA-RGD was added on the chamber microscope slides and incubated 90 min at 37°C. The tracer was removed, the chamber walls were removed, and cells were dip-washed twice with PBS. The slides were air dried for 10 minutes and exposed on a phosphor imaging plate (BAS-TR2025, Fuji Photo Film Co. Ltd., Tokyo, Japan) for 1 h. The distribution of radioactivity on the plate was visualized and quantified using a Fluorescent Image Analyzer (Fujifilm FLA-5100, Fuji Photo Film Co. Ltd., Tokyo, Japan).

#### 4.4.5 Immunohistochemical stainings (III)

After the measurements with gamma counter or autoradiography, the tissues were fixed in 70% ethanol for 15 min and stained with antibodies against von Willebrand factor (vWF) and collagen IV. The stained glasses were imaged, and the density of angiogenesis was visually evaluated and graded from 0 to 5.

### 4.5 Statistical analysis

All data are expressed as mean  $\pm$  SD. Statistical analysis was done with SPSS Statistics software v. 21 and v. 25 (IBM, NY, USA). In study I, receiver operating characteristic (ROC) analyses were performed, Youden index was used to obtain optimal cut-off values for [<sup>15</sup>O]water PET in comparison to TTC staining and the method of DeLong was used to compare area under the curve (AUC) values (DeLong et al., 1988). A paired Student's t test was applied for the comparisons of the

[<sup>68</sup>Ga]NODAGA-RGD uptake between ischaemic and remote areas. Comparisons of viable ischaemic, injured ischaemic and remote areas were done using ANOVA with Dunnett's correction for remote group. Comparisons of different vessel densities were done using ANOVA with Bonferroni correction. A Pearson's rank test (r) was used to analyse correlation between *ex vivo* autoradiography and  $\alpha_v\beta_3$  integrin immunohistochemistry and Spearman's rank test was used to analyse correlation between *in vitro* autoradiography and angiogenesis vessel density. p values less than 0.05 were considered statistically significant.

# 5 Results

## 5.1 Imaging of myocardial blood flow and viability (I)

### 5.1.1 MBF and PTF in MI

According to circumferential profile analysis, transmural infarction showed lower absolute MBF, relative MBF and PTF than remote myocardium ( $0.45 \pm 0.34$  vs.  $1.23 \pm 0.47$ ,  $p < 0.001$ ;  $0.37 \pm 0.23$  vs.  $0.99 \pm 0.014$ ,  $p < 0.001$ ; and  $0.55 \pm 0.12$  vs.  $0.84 \pm 0.11$ ,  $p < 0.001$ , respectively). Segmental absolute MBF, relative MBF and PTF by [ $^{15}\text{O}$ ]water PET decreased with increasing infarct volume fraction defined by TTC.

When the thickness of the ROI was increased, the PTF values decreased. The difference between small and large ROI thickness was  $12\% \pm 6\%$  ( $p < 0.001$ ) in segments with infarct volume fraction of  $< 75\%$ , and  $13\% \pm 10\%$  ( $p = 0.29$ ) in segments with transmural infarction. The ROI thickness had no effect on absolute or relative MBF.

### 5.1.2 Detection of infarction

ROC analysis of segmental relative MBF and PTF by [ $^{15}\text{O}$ ]water PET showed that relative MBF was more accurate than PTF in detecting any MI (segments with any infarction vs. no infarction) (AUC 0.76 vs. 0.68,  $p = 0.04$ ). Relative MBF of  $\leq 85\%$  and PTF of  $\leq 70\%$  were the optimal cut-off values for the detection of any MI. These cut-off values demonstrated modest sensitivity, but high specificity and positive predictive value (Table 4).

**Table 4** Performance of segmental relative myocardial blood flow (Rel MBF) and perfusable tissue fraction (PTF) by [<sup>15</sup>O]water PET in the detection of myocardial infarction.

No infarction vs. any infarction					
	Sensitivity	Specificity	Positive predictive value	Negative predictive value	Accuracy
Rel MBF (cut off ≤ 85%)	61%	84%	80%	67%	72%
PTF (cut off ≤ 70%)	54%	79%	76%	61%	66%

Relative MBF performed better than PTF (AUC 0.71 vs. 0.57,  $p = 0.004$ ) in the detection of subendocardial infarction (segments with infarct volume fraction 1%-49% vs. no infarction). There was no difference, however, between relative MBF and PTF in the detection of non-viable tissue defined as infarct volume fraction  $\geq 75\%$  (AUC 0.90 vs. 0.89,  $p = 0.89$ ).

The average size of the transmural MI was  $29\% \pm 15\%$  of the LV measured by relative MBF and  $29\% \pm 22\%$  of the LV measured by PTF ( $p = 0.99$ ) with the cut-off values derived from the ROC curve analysis.

### 5.1.3 Assessment of viability

The recovery of function with the infarct volume fraction of 50-75% is not distinct and, therefore, two definitions of viability were tested. When the segments with infarct volume fraction of  $< 50\%$  were defined as viable and segments with infarct volume fraction of  $\geq 50\%$  as non-viable, the ROC analysis showed AUC of 0.81 with relative MBF and 0.81 with PTF for the detection of viability ( $p = 0.97$ ) (Figure 4. A). The optimal cut-off values for relative MBF and PTF were  $\geq 79\%$  and  $\geq 66\%$ , respectively. These cut-off values showed similar sensitivities, specificities, and diagnostic accuracies for the detection of viability (Table 5). Segmental relative MBF and PTF were also compared with PTI for the detection of viability in a subset of pigs. The ROC analysis showed AUC of 0.81 with PTI and there was no difference between PTI and relative MBF ( $p = 0.41$ ) or PTF ( $p = 0.79$ ).

When the segments with infarct volume fraction of  $< 75\%$  were defined viable and segment with infarct volume fraction of  $\geq 75\%$  as non-viable, AUC of 0.85 with relative MBF and 0.86 with PTF ( $p = 0.77$ ) were found (Figure 4. B). The optimal cut-off values of  $\geq 67\%$  for relative MBF and  $\geq 66\%$  for PTF resulted in accuracies of 90% and 81%, respectively (Table 5). Comparison to PTI (AUC 0.9) showed no difference between PTI and relative MBF ( $p = 0.67$ ) or PTF ( $p = 0.50$ ). The optimal cut-off value of  $\geq 82\%$  of PTI yielded slightly better sensitivity, specificity, and diagnostic accuracy than those of relative MBF or PTF.

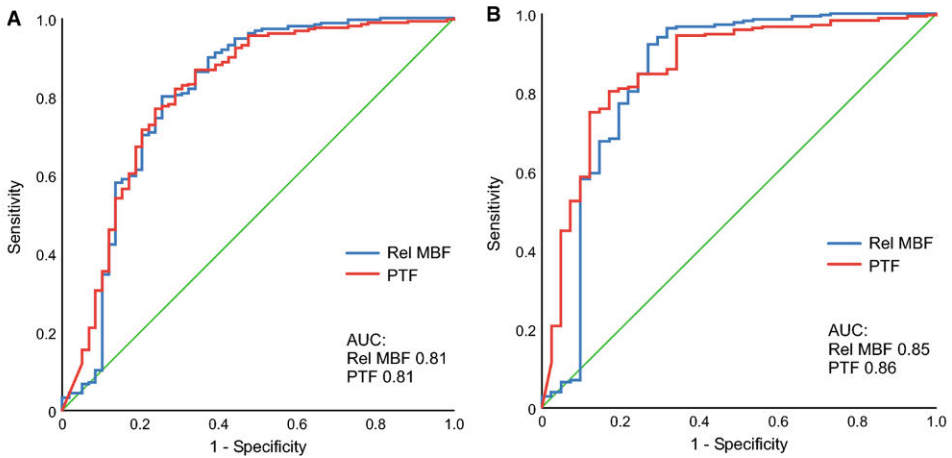


**Figure 4.** Receiver operating characteristics (ROC) curve analysis of relative myocardial blood flow (Rel MBF) and perfusable tissue fraction (PTF) by [ $^{15}\text{O}$ ]water in the detection of myocardial viability with infarct volume fraction of < 50% (A) and with infarct volume fraction of < 75% (B). From original publication I.

**Table 4.** Performance of segmental relative myocardial blood flow (Rel MBF) and perfusable tissue fraction (PTF) by [ $^{15}\text{O}$ ]water in the assessment of myocardial viability.

Viable tissue (infarct volume fraction < 50%)					
	Sensitivity	Specificity	Positive predictive value	Negative predictive value	Accuracy
Rel MBF (cut off $\geq$ 79%)	81%	69%	92%	46%	79%
PTF (cut off $\geq$ 66%)	82%	71%	92%	48%	80%
PTF (cut off $\geq$ 70%)	74%	76%	93%	41%	74%

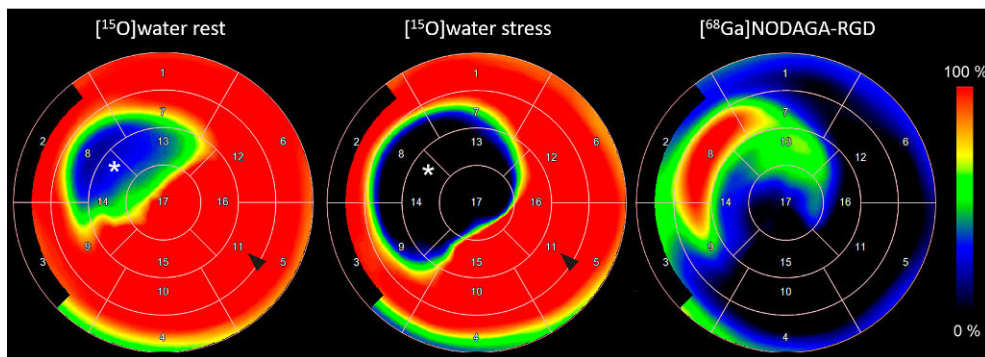
  

Viable tissue (infarct volume fraction < 75%)					
	Sensitivity	Specificity	Positive predictive value	Negative predictive value	Accuracy
Rel MBF (cut off $\geq$ 67%)	92%	73%	96%	59%	90%
PTF (cut off $\geq$ 66%)	80%	83%	97%	39%	81%
PTF (cut off $\geq$ 70%)	72%	88%	97%	32%	74%

## 5.2 Imaging of myocardial injury and angiogenesis (II and III)

### 5.2.1 [<sup>68</sup>Ga]NODAGA-RGD *in vivo* PET

The tracer activity in the blood pool remained higher than in the myocardium throughout the imaging session. Plasma protein binding study showed that the binding of [<sup>68</sup>Ga]NODAGA-RGD in the plasma proteins was low in all tested species. Plasma free fraction was  $0.94 \pm 0.011$  in the rat,  $0.93 \pm 0.017$  in the pig and  $0.91 \pm 0.081$  in the human serum. There was virtually no [<sup>68</sup>Ga]NODAGA-RGD uptake in the remote LV myocardium, whereas the uptake was regionally increased in the ischaemic area in all pigs (Figure 5). The average myocardial [<sup>68</sup>Ga]NODAGA-RGD uptake was higher in the ischaemic area than in the remote myocardium (SUV  $0.61 \pm 0.12$  vs.  $0.49 \pm 0.12$ ,  $p=0.003$ ).



**Figure 5.** Representative polar maps of MBF measured by [<sup>15</sup>O]water PET at rest and during adenosine stress and uptake of [<sup>68</sup>Ga]NODAGA-RGD. Increased [<sup>68</sup>Ga]NODAGA-RGD uptake is co-localised with an area of reduced myocardial perfusion (asterisks) as compared with the remote area (arrowhead). From original publication II.

### 5.2.2 Histology

Injured myocardium presented characteristic histological features of recent ischaemic myocardial injury including loose connective tissue with some mature collagen fibres. Myofibroblasts and inflammatory cells were abundant. In the viable ischaemic areas, the organisation of myocytes and connective tissue were normal, but some myocyte vacuolisation was seen. The immunohistochemical staining of CD31 showed no difference in the endothelial cell staining between remote, viable ischaemic and injured myocardium. The immunohistochemical staining of  $\alpha_v\beta_3$  integrin showed localised staining around the capillaries in the viable myocardium. The staining was diffuse in the injured myocardium and significantly higher, as



measured by areal percentage, than in the remote myocardium ( $23 \pm 1.9\%$  vs.  $7.5 \pm 1.0\%$ ,  $p < 0.001$ ). There was no difference between viable ischaemic myocardium and remote myocardium ( $10 \pm 4.0\%$  vs.  $7.5 \pm 1.0\%$ ,  $p = 0.15$ ). The  $\alpha$ -SMA staining was intense and, as measured by areal percentage, significantly higher in the injured myocardium than in the remote myocardium ( $7.2 \pm 2.9\%$  vs.  $1.3 \pm 0.75\%$ ,  $p = 0.019$ ).

### 5.2.3 *Ex vivo* experiments

#### 5.2.3.1 Biodistribution

The uptake of [ $^{68}\text{Ga}$ ]NODAGA-RGD was higher in the injured (TTC negative) myocardium in comparison to the remote myocardium (SUV  $0.79 \pm 0.21$  vs.  $0.49 \pm 0.21$ ,  $p = 0.016$ ). There was, however, no difference between the viable ischaemic (TTC positive) and remote myocardium (SUV  $0.49 \pm 0.17$  vs.  $0.49 \pm 0.21$ ,  $p = 0.99$ ).

#### 5.2.3.2 Autoradiography

Autoradiographs showed significantly higher [ $^{68}\text{Ga}$ ]NODAGA-RGD uptake in the injured than in the remote myocardium ( $4.6 \pm 2.1$  vs.  $1.8 \pm 0.61$  PSL/ $\text{mm}^2$ ,  $p = 0.006$ ). The uptake in the viable ischaemic myocardium was similar than in the remote myocardium ( $2.2 \pm 0.85$ ,  $p = 0.82$ ). The [ $^{68}\text{Ga}$ ]NODAGA-RGD measured by autoradiography positively correlated to the area percentage of  $\alpha_v\beta_3$  integrin staining in the tissue sections ( $r_{\text{Pearson}} = 0.73$ ,  $p = 0.0013$ ).

### 5.2.4 *In vitro* experiments

#### 5.2.4.1 *In vitro* tracer binding

The tracer binding study was performed for human cell derived angiogenesis tissue model with four different concentration of angiogenesis promoting growth factors. The tracer uptake measured by gamma counter gradually increased with increasing density of angiogenesis (Figure 6A-D). When compared to the control cells that were not treated with growth factors, the uptake of [ $^{68}\text{Ga}$ ]NODAGA-RGD was 1.6-fold higher with 25% growth factor concentration, 2.1-fold higher with 50%, 2.4-fold higher with 75% and 2.5-fold higher with 100% growth factor concentration. In comparison to the growth factor concentration of 25%, the uptake of [ $^{68}\text{Ga}$ ]NODAGA-RGD was significantly higher with the 75% and 100% growth factor concentrations (Figure 6E). The [ $^{68}\text{Ga}$ ]NODAGA-RGD uptake correlated with the amount of angiogenesis visually evaluated from histological stainings (Figure 6F).

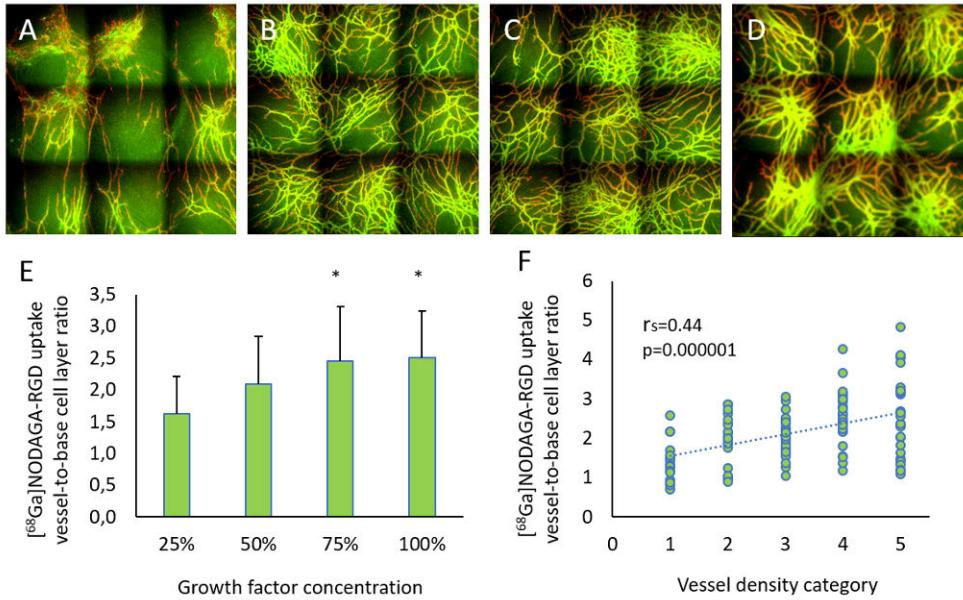


**Figure 6.** Representative images of the tubule networks with different growth factor concentrations: 25% (A), 50% (B), 75% (C) and 100% (D) stained with von Willebrand factor (red) and collagen IV (green) antibodies. The graph in E shows the vessel-to-base cell layer ratio of  $[^{68}\text{Ga}]\text{NODAGA-RGD}$  uptake with different growth factor concentrations, and graph in F shows the correlation between the vessel density and the vessel-to-base cell layer ratio of  $[^{68}\text{Ga}]\text{NODAGA-RGD}$  uptake. From original publication III.

### 5.2.4.2 Autoradiography

Autoradiography was performed to vessels with growth factor concentrations of 75% and 100%. The uptake of  $[^{68}\text{Ga}]\text{NODAGA-RGD}$  was localized in the areas of angiogenesis and was significantly higher with 100% growth factor concentration in comparison to 75% growth factor concentration (vessel-to-base cell layer ratio  $3.3 \pm 0.09$  vs.  $2.5 \pm 0.63$ ,  $p = 0.009$ )

## 6 Discussion

### 6.1 Pig models of myocardial ischaemia and infarction

Pigs with a surgically or percutaneously induced myocardial ischaemia and infarction were used in this study. Pigs are well suited for translational cardiovascular research since they offer several advantages in comparison to other animal models. Pigs are almost identical to humans in relation to the heart and coronary artery blood supply. The heart weight-to-body weight ratio of pigs is comparable to that of humans enabling the use of clinical scanners and more reliable discrimination between the injured and normal myocardial areas. (Lelovas et al., 2014; Swindle et al., 2012)

The surgical model is relatively laborious to perform and uncomfortable for the animals but results in quite large MI (Tarkia et al., 2015; Teramoto et al., 2011). Stent implantation has been shown to immediately cause severe reduction in blood flow in the target coronary artery (Rissanen et al., 2013). The occlusion of the stent can be mediated by antiplatelet medication, which was continued throughout our studies. Despite the medication, injured myocardium was found in some of the stented pigs probably due to insufficient compensation for reduction in myocardial perfusion by collateral formation, occlusion of a side branch by the stent, or thrombosis within the stent.

The pigs used in our studies were three months old in the beginning of the studies. The CAD patients, however, are usually older and might have comorbidities limiting their capability to adapt to the ischaemia. Use of older pigs is not as feasible due to their growth rate, which can be avoided to some extent by using minipigs. Another limitation for using pigs is challenges in the handling of the animals due to their size and higher costs of the housing of the animals, especially if older, larger animals and long follow-up times are used.

Regarding the medications used in our studies, there are some limitations that should be acknowledged. We used propofol in maintaining the anaesthesia. Propofol is a vasorelaxant leading to a decrease in vascular resistance and arterial pressure without affecting the heart rate. It also might pose a challenge regarding interactions with stress agents used in perfusion studies. (Croteau et al., 2004). We used

adenosine as a pharmacologic stress agent. Pigs often have variable systemic haemodynamic responses to adenosine and the dose had to be adjusted in some pigs. Adenosine infusion was combined with  $\alpha_1$ -adrenoceptor agonist phenylephrine, which can be used to counteract the systemic effects of adenosine leaving the adenosine-induced coronary vasodilatation undisturbed (Rossi et al., 2013). Dipyridamole has been shown to provide stronger hyperemic response than adenosine in the heart of propofol-anaesthetised pig (Rasmussen et al., 2016b).

## 6.2 Imaging of myocardial blood flow and viability

Viable but dysfunctional myocardium has potential to regain contractile function after restoration of blood flow. Thus, the detection of viable myocardium, in addition to ischaemia, is clinically important in determining the patients with CAD who will most likely benefit from revascularisation. Several imaging techniques, such as echocardiography, MRI, SPECT, and PET, have been used to assess viable myocardium. Of these, [ $^{18}\text{F}$ ]FDG PET in combination with perfusion imaging is considered the most optimal technique. Also PTF and PTI by [ $^{15}\text{O}$ ]water PET have been shown to detect viability and predict functional recovery after MI (Bondarenko et al., 2011; Iida et al., 2012; Itoh et al., 2002; Timmer et al., 2017; Yamamoto et al., 1992). The detection of viability with resting MBF assessed by [ $^{15}\text{O}$ ]water PET, however, still remains incompletely studied. We evaluated the performance of resting relative MBF, PTF and PTI by [ $^{15}\text{O}$ ]water PET in the detection of MI and viability. Relative MBF, PTF and PTI were segmentally compared to histology.

Due to its optimal characteristics, [ $^{15}\text{O}$ ]water PET is considered the golden standard for perfusion imaging. In clinical practise, assessment of ischaemia and MI is normally performed with combined rest and stress imaging. Reduced resting MBF is a marker of an MI scar both in experimental models (Bol et al., 1993; Herrero et al., 1995; Iida et al., 1995) and in patients (de Silva et al., 1992; Gerber et al., 1998; Iida et al., 2012). We showed an MBF of  $0.45 \pm 0.34$  ml/g/min in the centre of transmural infarction which is in line with previous studies showing MBF values between 0.35 and 0.45 ml/g/min in necrotic areas (Bol et al., 1993; de Silva et al., 1992; Herrero et al., 1995). There was a gradual decrease of segmental absolute and relative MBF and PTF with increasing infarct volume fraction. Also, absolute and relative MBF were decreased in segments with any infarction, but PTF was lower only when the infarct volume fraction was  $\geq 50\%$ .

We also studied the effect of ROI thickness on the MBF and PTF. MBF is independent of ROI thickness (Iida et al., 1988) and, as expected, increasing the thickness of the ROI had no effect on absolute or relative MBF, whereas it resulted in a reduction of PTF. PTF is the fraction of tissue capable of rapidly exchanging [ $^{15}\text{O}$ ]water in a specific ROI. Increasing the thickness of the ROI decreases PTF

because more extramyocardial components are included in the ROI. As PTF is sensitive for variations, careful standardisation of ROI definition is required. PTI is the ratio of PTF and ATF which both decrease equally with increasing ROI thickness, and therefore, PTI will remain unaffected by changes in ROI thickness. (Knaapen et al., 2003) ATF is the mass of extravascular tissue in the ROI, and can be determined by blood-pool imaging with [ $^{15}\text{O}$ ]CO or a software-based calculation of parametric PTI images from single [ $^{15}\text{O}$ ]water scan (De Haan et al., 2012; Harms et al., 2011).

For the detection of viability defined as segments with infarct volume fraction < 75%, our study showed optimal cut-off values of  $\geq 67\%$  for relative MBF,  $\geq 66\%$  for PTF and  $\geq 82\%$  for PTI, which are in line with previous studies showing cut-off values of 70% for PTF and 85% for PTI (Bondarenko et al., 2011; De Haan et al., 2012). Previous literature has shown, however, variation between 70 and 85% in the cut-off values for PTI (De Haan et al., 2012; de Silva et al., 1992; Timmer et al., 2017). Although the cut-off value for the PTF determined by us was quite similar than previously reported, it resulted in lower diagnostic accuracy in our material. The ROC analysis showed AUC of 0.85, 0.86, and 0.90 for MBF, PTF, and PTI, respectively. Relative MBF showed high sensitivity for detecting viable segments, but the specificity was lower. This might be due to normal MBF in some areas of subendocardial infarction.

Accuracy of 79-90% with relative MBF in the detection of viability shown by us is higher or similar than with [ $^{18}\text{F}$ ]FDG PET (79%), dobutamine echocardiography (79%), [ $^{99\text{m}}\text{Tc}$ ]sestamibi SPECT (75%), [ $^{201}\text{Th}$ ] SPECT (71%), and MRI techniques (61%-78%) with the endpoint of improvement of regional function (Schinkel et al., 2004). Combination of [ $^{18}\text{F}$ ]FDG and perfusion PET is considered the best method to assess viability. It requires, however, two PET scans leading to longer imaging sessions and higher radiation burden for the patients. With [ $^{15}\text{O}$ ]water PET, the perfusion and viability could be assessed with the same imaging session. The clinical endpoint in viability studies is recovery of contractile function after revascularization which, in addition to cut-off values, needs to be evaluated in future clinical studies with patients. Our experimental study, however, shows that evaluation of viability by [ $^{15}\text{O}$ ]water PET is feasible.

We determined relative MBF by normalising the absolute MBF values for remote normal myocardium. The use of reference region and relative values, however, might be problematic in patients with multi-vessel disease and quantitative approach should be used. The cut-off values for relative rather than absolute MBF were, however, determined due to concerns related to species differences and effects of anaesthesia. Also, large variability in the resting global flow can often be seen in pigs with MI scar.

### 6.3 Imaging of myocardial injury and angiogenesis

The molecular processes taking place during infarct healing serve as potential biomarkers for the assessment of risk for developing LV remodelling and heart failure. Expression of  $\alpha_v\beta_3$  integrin is associated with several events during cardiac repair after myocardial infarction, including angiogenesis, regulation of macrophage inflammatory responses and myofibroblast differentiation (Antonov et al., 2011; Sarrazy et al., 2014; Sun et al., 2003). RGD-based  $\alpha_v\beta_3$  integrin targeted tracers detect increased  $\alpha_v\beta_3$  integrin expression after ischaemic myocardial injury in animal studies and in humans (Higuchi et al., 2008; Makowski et al., 2008; Meoli et al., 2004; Rasmussen et al., 2016a; Sun et al., 2014), and have shown potential to predict LV remodelling (Sherif et al., 2012) and functional recovery after revascularisation (Jenkins et al., 2016). [ $^{68}\text{Ga}$ ]NODAGA-RGD is a novel PET tracer that consists of a pentacyclic peptide binding moiety Arg-Gly-Asp-D-Tyr-Lys coupled with the gallium chelating agent NODAGA. The tracer precursor is commercially available in Good Manufacturing Practices (GMP) quality and the tracer has been tested for clinical use (Gnesin et al., 2017; Van Der Gucht et al., 2016). The synthesis of [ $^{68}\text{Ga}$ ]NODAGA-RGD is relatively easy and straightforward, and it has a good target specificity and favorable kinetics, dosimetry and safety profile (Buchegger et al., 2011; Knetsch et al., 2011).

[ $^{68}\text{Ga}$ ]NODAGA-RGD uptake has been shown to demonstrate  $\alpha_v\beta_3$  integrin expression in infarcted rat myocardium 1 week after coronary ligation (Laitinen et al., 2013), which is in line with our study showing that the [ $^{68}\text{Ga}$ ]NODAGA-RGD cardiac PET detected increased myocardial  $\alpha_v\beta_3$  integrin expression two weeks after the induction of flow-limiting coronary stenosis in pigs. The uptake of [ $^{68}\text{Ga}$ ]NODAGA-RGD was localised in the injured myocardium, but not in the viable ischaemic myocardium indicating that [ $^{68}\text{Ga}$ ]NODAGA-RGD is a potential tool in detecting areas of recent myocardial injury in the presence of chronic ischaemia and in evaluating patients with hibernating myocardium containing a mixture of viable ischaemic and injured myocardium (Elsasser et al., 1997).

The *in vivo* PET imaging showed an increased uptake of [ $^{68}\text{Ga}$ ]NODAGA-RGD in the ischaemic myocardium, but the *ex vivo* biodistribution and autoradiography showed that the uptake was localised in the irreversibly injured myocardium, but not in the viable myocardium within the ischaemic area. The immunohistochemical staining of  $\alpha_v\beta_3$  integrin confirmed the increased expression, which also correlated with the [ $^{68}\text{Ga}$ ]NODAGA-RGD uptake measured by autoradiography. We found no difference in the endothelial cell staining between the remote, viable ischaemic and infarcted myocardial areas, but the staining of  $\alpha$ -SMA showed myofibroblast differentiation in the infarcted areas. These results indicate that, instead of angiogenesis, the  $\alpha_v\beta_3$  integrin expression and [ $^{68}\text{Ga}$ ]NODAGA-RGD uptake reflected other processes related to scar formation. It has been shown that  $\alpha_v\beta_3$

integrins are, indeed, expressed on myofibroblasts (Hinz, 2006) and RGD tracer uptake after experimental MI has also been traced to myofibroblasts (van den Borne et al., 2008). Angiogenesis and RGD tracer uptake have previously been shown to take place in severely hypoxic tissue (Dobrucki et al., 2009; Kalinowski et al., 2008). The severity and duration of ischaemia in our pig model, however, may not have been enough to induce angiogenesis. The  $\alpha_v\beta_3$  integrin expression and RGD uptake peak between 1 and 4 weeks after an ischaemic insult (Higuchi et al., 2008; Kiugel et al., 2014; Meoli et al., 2004; Sun et al., 2003). We chose the time point of 2 weeks for our study according to this, and the lack of other time points is a limitation. Previously, a direct correlation between the amount of endothelial cell staining and uptake of dimeric [ $^{68}\text{Ga}$ ]DOTA-RGD tracer has been shown at 4 weeks after MI indicating increased angiogenesis in the later stages of scar formation (Kiugel et al., 2014). Our study is, however, in line with a previous study in a pig model of myocardial hibernation where no angiogenesis or uptake of RGD was found (Johnson et al., 2008).

Since the expression of  $\alpha_v\beta_3$  integrin and uptake of RGD tracers also reflect other processes than angiogenesis in infarcted myocardium, we studied the [ $^{68}\text{Ga}$ ]NODAGA-RGD binding in an human cell based angiogenesis tissue model, which is devoid of most other RGD binding targets, such as macrophages. This *in vitro* study showed that the [ $^{68}\text{Ga}$ ]NODAGA-RGD binding is proportional to the amount of angiogenesis. However, when performing *in vivo* imaging studies of angiogenesis, possibility of nonspecific binding should be acknowledged.

The vessels in the tissue model have previously been shown to be covered by pericytes (Huttala et al., 2015; Sarkanen et al., 2011; Toimela et al., 2017). Pericyte coverage is characteristic to maturation of newly formed vessels in myocardium after infarction (Kobayashi et al., 2017) indicating that the model used here represents well the post-infarction angiogenesis. The  $\alpha_v\beta_3$  integrin also seems to be involved in the maturation of the vessels as anti- $\alpha_v\beta_3$  integrin therapy has been shown to decrease pericyte coverage in tumor vessels (Reinmuth et al., 2003).

One of the limitations in this study is the fact that the effect of therapeutic angiogenesis on [ $^{68}\text{Ga}$ ]NODAGA-RGD uptake was not tested. The possibility to monitor the response to angiogenic gene therapy with targeted PET tracers is intriguing. Previously, RGD-based tracers [ $^{123}\text{I}$ ]Gluco-RGD and [ $^{18}\text{F}$ ]alfatide II ([ $^{18}\text{F}$ ]AIF-NOTA-E[PEG4-c(RGDfk)]<sub>2</sub>) have been shown to detect gene therapy induced angiogenesis in hibernating pig myocardium (Johnson et al., 2008) and in rats after MI (Cai et al., 2016), respectively.

For logistic reasons, two different PET/CT scanners for [ $^{15}\text{O}$ ]water and [ $^{68}\text{Ga}$ ]NODAGA-RGD imaging were used. This might have affected the accuracy of the co-registration of the images. Also, respiratory and cardiac motion may affect sensitivity of [ $^{68}\text{Ga}$ ]NODAGA-RGD due to activity in the closely associated blood

pool in which the tracer uptake remained higher than the myocardial uptake throughout the imaging session. No clear explanation for the persistent high blood uptake in our pig model was found. There were no species differences in the binding of the tracer to plasma proteins between pigs, rats, and humans. Low amounts of  $\alpha_v\beta_3$  integrin, however, can be found on platelets (Bennett et al., 2009). Platelet count in pigs is much higher than that of humans (Chen et al., 2011) resulting in higher amount of  $\alpha_v\beta_3$  integrin in blood and possibly explaining the higher blood radioactivity in pigs than in human.

## 6.4 Future directions

Molecular imaging with PET is a valuable tool in the discovery and initial evaluation of new therapies and in the diagnostics and risk stratification of patients. PET imaging of biological processes involved in the healing of MI and LV remodelling could be used as prognostic markers in identifying patients at high risk for developing HF, and in the evaluation of the efficacy of new therapies (Saraste & Knuuti, 2017).

[ $^{15}\text{O}$ ]water PET is well established for the detection of CAD (Driessen et al., 2017). Our results show that [ $^{15}\text{O}$ ]water PET is a potential tool in the detection of viability. This was, however, an animal study and the cut-off values need to be determined in patients. Functional recovery after revascularisation is most used clinical end point in viability studies (Schinkel et al., 2007), and should be evaluated in future clinical studies of viability assessment using [ $^{15}\text{O}$ ]water PET. Also, direct comparison of [ $^{15}\text{O}$ ]water PET with some other techniques or tracers, such as [ $^{18}\text{F}$ ]FGD for viability assessment would be of interest.

Different characteristics during infarct healing and LV remodelling serve as potential biomarkers for the detection and risk stratification of HF. Several new tracers for the detection of angiogenesis after MI to predict LV remodelling and development of HF have been studied, also in patients (Jenkins et al., 2016), but none are yet in routine clinical use. The prognosis of HF is poor as half of the patients with HF die in five years (Mcmurray & Pfeffer, 2004). Thus, new, and more effective therapies, such as angiogenic gene therapy are needed for the treatment of these patients. Monitoring of the therapy response to angiogenic gene therapy has, so far, been done for example with perfusion imaging (Hartikainen et al., 2017). It would, however, be of interest to directly detect the amount of neoangiogenesis in the treatment area. RGD based tracers, such as [ $^{68}\text{Ga}$ ]NODAGA-RGD are potential tools for this purpose. The tracer already has been studied in humans with cancer (Van Der Gucht et al., 2016) and carotid artery disease (Gnesin et al., 2017), and studies with MI patients are ongoing. Our results showed that RGD uptake correlated with the amount of angiogenesis *in vitro*, but more studies are still needed to determine to



which extent the in vivo uptake of RGD based tracers is from angiogenesis and to which extent from other possible targets with increased  $\alpha\beta3$  integrin expression, such as myofibroblasts and macrophages.

# 7 Conclusions

This study evaluated PET tracers for the detection of myocardial viability and repair process after MI. The main findings and conclusions of the studies I-III are following:

1. Resting MBF, PTF, and PTI based on [ $^{15}\text{O}$ ]water PET perfusion imaging detected myocardial viability with good accuracy.
2. [ $^{68}\text{Ga}$ ]NODAGA-RGD PET demonstrated increased myocardial  $\alpha_v\beta_3$  integrin expression in a pig model of coronary stenosis. The uptake of [ $^{68}\text{Ga}$ ]NODAGA-RGD was localised in the irreversibly injured myocardium.
3. [ $^{68}\text{Ga}$ ]NODAGA-RGD binding was proportional to the amount of angiogenesis in an *in vitro* 3D model of angiogenesis.

Resting MBF, PTF and PTI based on [ $^{15}\text{O}$ ]water PET perfusion imaging are useful for the assessment of myocardial viability. [ $^{68}\text{Ga}$ ]NODAGA-RGD PET may be useful for the identification of  $\alpha_v\beta_3$  integrin activation associated with repair of myocardial injury.

# Acknowledgements

This study was carried out in the Turku PET Centre and the Department of Clinical Physiology and Nuclear Medicine in Turku University Hospital and the University of Turku. It has been a privilege to work in the Turku PET Centre and I wish to express my gratitude to Professor Juhani Knuuti, Director of Turku PET Centre, Professor Jaakko Hartiala, Head of the Department of Clinical Physiology and Nuclear Medicine during the first years of this thesis, and Professor Jukka Kempainen, Head of the Department of Clinical Physiology and Nuclear Medicine since May 2016, for providing top notch facilities and technology for the research.

I owe my deepest heartfelt gratitude to my supervisors Associate Professor Antti Saraste and Professor Anne Roivainen. Antti, thank you for giving me the opportunity to start the PhD project in the cardiac imaging group. You have given me space, yet you have always been available when I have needed guidance. Your amazingly positive attitude and encouragement have pulled me from despair several times when I have lost my motivation. Anne, your attention to detail and vast understanding and experience in preclinical imaging have been essential for this work. I thank you for the relaxed atmosphere in the group meetings and that your door has always been open for your students. I also want to thank both of you for all the financial support that I would not have survived without. I also want to express my gratitude to Juhani for so many good insights regarding the studies and for financial support.

I am most grateful to the reviewers of this thesis, Adjunct Professor Riikka Kivelä and Adjunct Professor Jens Sörensen for your time and valuable comments which helped me to improve this thesis. I also thank the members of my follow-up committee, Professor Juhani Knuuti, Professor Seppo Ylä-Herttuala and Adjunct Professor Tuomas Kiviniemi for all the guidance during this process. Seppo is also thanked for a fruitful collaboration between Turku and Kuopio, and Tuomas for supportive and constructive commenting of the manuscripts.

I wish to thank Professor Mika Scheinin, Director of FinPharmaNet, Professor Markku Koulu and Associate Professor Eriika Savontaus, past and present directors of Drug Research Doctoral Programme (DRDP), University of Turku for providing excellent education and annual meetings for PhD students. I also thank Eeva Valve,

the coordinator of DRDP for all the help and support regarding the doctoral studies during these years.

These studies are a result of teamwork and I could never have done any of this without the help from others. I wish to thank all the co-authors and collaborators for invaluable contribution to the studies. Especially, I thank Miikka Tarkia for fun moments in the lab and for teaching me all the practical issues related to pigs and imaging studies. You sure left big shoes for me to fill. I thank Timo Savunen for your expertise and mentoring in the pig studies. Paavo Halonen and Antti Kuivanen are thanked for contribution to the studies, and with Jussi Nurro and Olli-Pekka Hätinén, for memorable moments and bad humour in the pig house. Tuomas Kiviniemi, Christoffer Stark, Tommi Vähäsilta and Mikko Pietilä are thanked for contribution to the pig experiments in Turku, Mark Lubberink is thanked for expertise in analysing cardiac images, and Pekka Saukko for pathological expertise. I thank Virva Saunavaara, Jarmo Teuho, Mika Teräs and Tuula Tolvanen for carrying out the imaging studies and Meeri Käkälä, Olli Metsälä, Olli Moisio and Xiang-Guo Li for performing  $^{68}\text{Ga}$ -syntheses. I truly have enjoyed working with you. Tarja Toimela, Outi Huttala and Tuula Heinonen are thanked for collaboration during the *in vitro* angiogenesis study. Your expertise was essential and your flexibility in meeting all our needs made this study possible.

I thank the personnel of the PET Centre for a nice atmosphere in the lab and in the coffee room. Especially, warm thanks go to Nanna Liukko-Sipi, Emilia Puhakka and Sanna Suominen for providing radiowater for our studies outside office hours, and for creating a nice atmosphere in the lab during all those long evenings and weekends. Aake Honkaniemi and Minna Aatsinki are thanked for the scheduling, which was usually asked with a very short notice. Mirja Jyrkinen, Lenita Saloranta and Auli Kärpijoki are thanked for helping with all the secretarial matters. Warm thanks go to Carimas guys Sauli Pirola and Timo Laitinen for creating new plug-ins on demand. They have been essential for our analyses. Marko Tättäläinen and Rami Mikkola are acknowledged for the help with IT issues.

I warmly thank the staff of the Central Animal Laboratory of the University of Turku for great amount of help with the pig studies and for taking good care of the pigs. I also wish to acknowledge Liisa Lempiäinen and Erica Nyman for performing immunohistochemistry.

I want to thank the past and present group members: Anu, Andriana, Arina, Heidi, Helena, Jenni, Johanna, Max, Max, Mia, Miikka, Olli, Petri, Reija, Riikka, Senthil and Sanna. Even though I have not had common projects with most of you, we have shared the office and the journey. Your peer support, coffee break company, humour and friendship have been very important during these years. Especially, I want to thank Helena for friendship and for helping me to carry on when it was most difficult.

I also want to express my gratitude to my Pro gradu supervisor Irma Holopainen and the Hippo-group for giving me the basis for the scientific work. I am happy that we still, from time to time, meet over dinner and catch up.

I am blessed to have so many wonderful friends who have helped me put the life and thesis in perspective. I want to thank the Farmis girls Anna-Maija, Henriikka, Laura, Minttu, Noora and Satu for being amazing friends and for an invaluable peer support in science and in life. Nowadays we are rarely all gathered at the same time, but whatever the squad, I always look forward to our next meeting. I thank the Pori girls Eve, Hanna, Johanna, Milla, Nelli, Reetta and Tuija for your friendship since childhood. With all the spouses and kids, we are quite a gang! We have shared joy and sorrow during the decades, and I can say that you are the friends that truly know me the best. With you the life is full of laughter and singing. Special thanks go to Hanna, my partner in crime throughout the years. I thank Aurora, Olli, and the kids for keeping us in Turku. Your friendship has been invaluable during these years and I have enjoyed every moment and all the culinary adventures with you. I also thank skate mom Riikka for friendship, humour, and never-ending phone calls.

I wish to thank my parents-in-law Sinikka and Matti, and Taina, Tuija and Henrik with your spouses and families for taking me as a member of the Grönman family and for love, support, and friendship. I thank my grandmother Mary for love and for the keen interest towards my work. I am most grateful to my parents Seija and Juha for the best possible environment to grow in and for all the love and encouragement that you have given me. You have always been there to support and push me forward. Also, I thank you for helping with the kids and the numerous trips that you have taken them to. I thank my sisters Essi, Katri and Sara for wonderful memories from childhood and for your friendship. I also thank my brothers-in-law Harri, Topias and Mika for the friendship and all the nice moments throughout the years, and Aaro for all the action. In our crazy extended family, there has never been a lack of weird humour and loud, lively conversations.

Finally, the greatest thanks go to my family. Armi and Artturi, it has been wonderful to see you grow to be such smart, brilliant teenagers. I am so proud of you two and love you more than I can describe. And most of all, I thank Jussi, love of my life, my everything. Thank you for always being there and keeping my feet on the ground when my head flies in the clouds. You truly are my better half and I look forward to our next adventures in life. MRS

These studies were conducted within the Finnish Centre of Excellence in Cardiovascular and Metabolic Diseases supported by the Academy of Finland, University of Turku, Turku University Hospital and Åbo Akademi University. This study was financially supported by the Drug Research Doctoral Programme, University of Turku Graduate School, and the Hospital District of Southwest Finland/Turku University Hospital (EVO/ERVA grant). Grants were also obtained

Maria Grönman

from Ida Montin's foundation, Maud Kuistila Memorial foundation, and Orion Research foundation. Drug Research Doctoral Programme, Finnish Isotope society, and Turku University foundation are acknowledged for providing travel grants.

Turku, August 2020

A handwritten signature in black ink, appearing to read 'Maria Grönman', with a large, stylized flourish at the end.

*Maria Grönman*

# References

- Andrassy, M., Volz, H. C., Igwe, J. C., Funke, B., Eichberger, S. N., Kaya, Z., Buss, S., Autschbach, F., Pleger, S. T., Lukic, I. K., Bea, F., Hardt, S. E., Humpert, P. M., Bianchi, M. E., Mairbörl, H., Nawroth, P. P., Remppis, A., Katus, H. A., & Bierhaus, A. (2008). High-mobility group box-1 in ischemia-reperfusion injury of the heart. *Circulation*, *117*(25), 3216–3226. <https://doi.org/10.1161/CIRCULATIONAHA.108.769331>
- Antonov, A. S., Antonova, G. N., Munn, D. H., Mivechi, N., Lucas, R., Catravas, J. D., & Verin, A. D. (2011).  $\alpha V\beta 3$  integrin regulates macrophage inflammatory responses via PI3 kinase/Akt-dependent NF- $\kappa$ B activation. *Journal of Cellular Physiology*, *226*(2), 469–476. <https://doi.org/10.1002/jcp.22356>
- Arslan, F., de Kleijn, D. P., & Pasterkamp, G. (2011). Innate immune signaling in cardiac ischemia. *Nature Reviews Cardiology*, *8*(5), 292–300. <https://doi.org/10.1038/nrcardio.2011.38>
- Bax, J. J., & Delgado, V. (2015). Myocardial viability as integral part of the diagnostic and therapeutic approach to ischemic heart failure. *Journal of Nuclear Cardiology: Official Publication of the American Society of Nuclear Cardiology*, *22*(2), 229–245. <https://doi.org/10.1007/s12350-015-0096-5>
- Bax, J. J., Patton, J. A., Pldermans, D., Elhendy, A., & Sandler, M. P. (2000). 18-Fluorodeoxyglucose imaging with positron emission tomography and single photon emission computed tomography: Cardiac applications. *Seminars in Nuclear Medicine*, *30*(4), 281–298. <https://doi.org/10.1053/snuc.2000.9543>
- Bennett, J. S., Berger, B. W., & Billings, P. C. (2009). The structure and function of platelet integrins. *Journal of Thrombosis and Haemostasis: JTH*, *7 Suppl 1*, 200–205. <https://doi.org/10.1111/j.1538-7836.2009.03378.x>
- Berman, D., Maddahi, J., Tamarappoo, B. K., Czernin, J., Taillefer, R., Udelson, J., Gibson, M., Devine, M., Lazewatsky, J., Bhat, G., & Washburn, D. (2013). Flurpiridaz F 18 PET: Phase II Safety and Clinical Comparison with SPECT Myocardial Perfusion Imaging for Detection of Coronary Artery Disease. *JACC*, *61*(4), 469–477. <https://doi.org/10.1038/jid.2014.371>
- Bleumink, G., Knetsch, A., Sturkenboom, M., Straus, S., Hofman, A., Deckers, J., Wittteman, J., & Stricker, B. (2004). Quantifying the heart failure epidemic: prevalence, incidence rate, lifetime risk and prognosis of heart failure: The Rotterdam Study. *European Heart Journal*, *25*(18), 1614–1619. <https://doi.org/10.1016/j.ehj.2004.06.038>
- Bol, A., Melin, J. A., Vanoverschelde, J. L., Baudhuin, T., Vogelaers, D., De Pauw, M., Michel, C., Luxen, A., Labar, D., & Cogneau, M. (1993). Direct comparison of [ $^{13}\text{N}$ ]ammonia and [ $^{15}\text{O}$ ]water estimates of perfusion with quantification of regional myocardial blood flow by microspheres. *Circulation*, *87*(2), 512–525. <http://www.ncbi.nlm.nih.gov/pubmed/8425298>
- Bondarenko, O., Knaapen, P., Beek, A. M., Boellaard, R., Lammertsma, A. A., & Van Rossum, A. C. (2011). Prediction of functional recovery after revascularization in patients with chronic ischemic myocardial dysfunction: perfusable tissue index by positron emission tomography and contrast-enhanced MRI comparison study. *Nucl Med Commun Wolters Kluwer Health Nuclear Medicine Communications*, *32*(32). <https://doi.org/10.1097/MNM.0b013e32834bfe51>

- Brooks, P. C., Clark, R. A., & Cheresh, D. A. (1994). Requirement of vascular integrin alpha v beta 3 for angiogenesis. *Science (New York, N.Y.)*, *264*(5158), 569–571. <http://www.ncbi.nlm.nih.gov/pubmed/7512751>
- Buchegger, F., Viertl, D., Baechler, S., Dunet, V., Kosinski, M., Poitry-Yamate, C., Rüegg, C., & Prior, J. O. (2011). <sup>68</sup>Ga-NODAGA-RGDyK for αvβ3 integrin PET imaging. *Nuklearmedizin*, *50*(6), 225–233. <https://doi.org/10.3413/Nukmed-0416-11-06>
- Cademartiri, F., Seitun, S., Clemente, A., La Grutta, L., Toia, P., Runza, G., Midiri, M., & Maffei, E. (2017). Myocardial blood flow quantification for evaluation of coronary artery disease by computed tomography. *Cardiovascular Diagnosis and Therapy*, *7*(2), 129–150. <https://doi.org/10.21037/cdt.2017.03.22>
- Cai, M., Ren, L., Yin, X., Guo, Z., Li, Y., He, T., Tang, Y., Long, T., Liu, Y., Liu, G., Zhang, X., & Hu, S. (2016). PET monitoring angiogenesis of infarcted myocardium after treatment with vascular endothelial growth factor and bone marrow mesenchymal stem cells. *Amino Acids*, *48*(3), 811–820. <https://doi.org/10.1007/s00726-015-2129-4>
- Caner, B., & Beller, G. A. (1998). Are technetium-99m-labeled myocardial perfusion agents adequate for detection of myocardial viability? *Clinical Cardiology*, *21*(4), 235–242. <http://www.ncbi.nlm.nih.gov/pubmed/9562932>
- Carmeliet, P., & Jain, R. K. (2011). Molecular mechanisms and clinical applications of angiogenesis. *Nature*, *473*(7347), 298–307. <https://doi.org/10.1038/nature10144>
- Chareonthaitawee, P., Christian, T. F., Hirose, K., Gibbons, R. J., & Rumberger, J. A. (1995). Relation of initial infarct size to extent of left ventricular remodeling in the year after acute myocardial infarction. *Journal of the American College of Cardiology*, *25*(3), 567–573. [https://doi.org/10.1016/0735-1097\(94\)00431-O](https://doi.org/10.1016/0735-1097(94)00431-O)
- Chen, Y., Qin, S., Ding, Y., Li, S., Yang, G., Zhang, J., Li, Y., Cheng, J., & Lu, Y. (2011). Reference values of biochemical and hematological parameters for Guizhou minipigs. *Experimental Biology and Medicine (Maywood, N.J.)*, *236*(4), 477–482. <https://doi.org/10.1258/ebm.2011.010283>
- Cochain, C., Channon, K. M., & Silvestre, J.-S. (2013). Angiogenesis in the Infarcted Myocardium. *Antioxidants & Redox Signaling*, *18*(9), 1100–1113. <https://doi.org/10.1089/ars.2012.4849>
- Coelho-Filho, O. R., Rickers, C., Kwong, R. Y., & Jerosch-Herold, M. (2013). MR Myocardial Perfusion Imaging. *Radiology*, *266*(3), 701–715. <https://doi.org/10.1148/radiol.12110918>
- Croteau, E., Bénard, F., Bentourkia, M., Rousseau, J., Paquette, M., & Lecomte, R. (2004). Quantitative myocardial perfusion and coronary reserve in rats with <sup>13</sup>N-ammonia and small animal PET: Impact of anesthesia and pharmacologic stress agents. *Journal of Nuclear Medicine*, *45*(11), 1924–1930.
- Cwajg, J. M., Cwajg, E., Nagueh, S. F., He, Z. X., Qureshi, U., Olmos, L. I., Quinones, M. A., Verani, M. S., Winters, W. L., & Zoghbi, W. A. (2000). End-diastolic wall thickness as a predictor of recovery of function in myocardial hibernation. *Journal of the American College of Cardiology*, *35*(5), 1152–1161. [https://doi.org/10.1016/S0735-1097\(00\)00525-8](https://doi.org/10.1016/S0735-1097(00)00525-8)
- Danad, I., Raijmakers, P. G., Driessen, R. S., Leipsic, J., Raju, R., Naoum, C., Knuuti, J., Mäki, M., Underwood, R. S., Min, J. K., Elmore, K., Stuijzfand, W. J., van Royen, N., Tulevski, I. I., Somsen, A. G., Huisman, M. C., van Lingem, A. A., Heymans, M. W., van de Ven, P. M., ... Knaapen, P. (2017). Comparison of Coronary CT Angiography, SPECT, PET, and Hybrid Imaging for Diagnosis of Ischemic Heart Disease Determined by Fractional Flow Reserve. *JAMA Cardiology*, *2*(10), 1100. <https://doi.org/10.1001/jamacardio.2017.2471>
- Danad, I., Uusitalo, V., Kero, T., Saraste, A., Raijmakers, P. G., Lammertsma, A. A., Heymans, M. W., Kajander, S. A., Pietilä, M., James, S., Sörensen, J., Knaapen, P., & Knuuti, J. (2014). Quantitative Assessment of Myocardial Perfusion in the Detection of Significant Coronary Artery Disease: Cutoff Values and Diagnostic Accuracy of Quantitative [<sup>15</sup>O]H<sub>2</sub>O PET Imaging. *Journal of the American College of Cardiology*, *64*(14), 1464–1475. <https://doi.org/10.1016/J.JACC.2014.05.069>



- De Haan, S., Harms, H. J., Lubberink, M., Allaart, C. P., Danad, I., Chen, W. J. Y., Diamant, M., Van Rossum, A. C., Iida, H., Lammertsma, A. A., & Knaapen, P. (2012). Parametric imaging of myocardial viability using 15O-labelled water and PET/CT: Comparison with late gadolinium-enhanced CMR. *European Journal of Nuclear Medicine and Molecular Imaging*, 39(8), 1240–1245. <https://doi.org/10.1007/s00259-012-2134-8>
- de Silva, R., Yamamoto, Y., Rhodes, C. G., Iida, H., Nihoyannopoulos, P., Davies, G. J., Lammertsma, A. A., Jones, T., & Maseri, A. (1992). Preoperative prediction of the outcome of coronary revascularization using positron emission tomography. *Circulation*, 86(6), 1738–1742. <http://www.ncbi.nlm.nih.gov/pubmed/1451245>
- DeLong, E. R., DeLong, D. M., & Clarke-Pearson, D. L. (1988). Comparing the areas under two or more correlated receiver operating characteristic curves: a nonparametric approach. *Biometrics*, 44(3), 837–845. <http://www.ncbi.nlm.nih.gov/pubmed/3203132>
- Depre, C., Kim, S.-J., John, A. S., Huang, Y., Rimoldi, O. E., Pepper, J. R., Dreyfus, G. D., Gaussin, V., Pennell, D. J., Vatner, D. E., Camici, P. G., & Vatner, S. F. (2004). Program of cell survival underlying human and experimental hibernating myocardium. *Circulation Research*, 95(4), 433–440. <https://doi.org/10.1161/01.RES.0000138301.42713.18>
- Dilsizian, V., Eckelman, W. C., Loreda, M. L., Jagoda, E. M., & Shirani, J. (2007). Evidence for tissue angiotensin-converting enzyme in explanted hearts of ischemic cardiomyopathy using targeted radiotracer technique. *Journal of Nuclear Medicine: Official Publication, Society of Nuclear Medicine*, 48(2), 182–187. <http://www.ncbi.nlm.nih.gov/pubmed/17268012>
- Dobaczewski, M., Gonzalez-Quesada, C., & Frangogiannis, N. (2010). The extracellular matrix as a modulator of the inflammatory and reparative response following myocardial infarction. *Journal of Molecular and Cellular Cardiology*, 48(3), 504–511. <https://doi.org/10.1016/j.jmcc.2009.07.015>
- Dobrucki, L. W., Meoli, D. F., Hu, J., Sadeghi, M. M., & Sinusas, a. J. (2009). Regional hypoxia correlates with the uptake of a radiolabeled targeted marker of angiogenesis in rat model of myocardial hypertrophy and ischemic injury. *Journal of Physiology and Pharmacology: An Official Journal of the Polish Physiological Society*, 60 Suppl 4, 117–123.
- Driessen, R. S., Raijmakers, P. G., Stuijzand, W. J., & Knaapen, P. (2017). Myocardial perfusion imaging with PET. *The International Journal of Cardiovascular Imaging*, 33(7), 1021–1031. <https://doi.org/10.1007/s10554-017-1084-4>
- Elsasser, A., Schlepper, M., Klovekorn, W.-P., Cai, W.-J., Zimmermann, R., Muller, K.-D., Strasser, R., Kostin, S., Gagel, C., Munkel, B., Schaper, W., & Schaper, J. (1997). Hibernating Myocardium: An Incomplete Adaptation to Ischemia. *Circulation*, 96(9), 2920–2931. <https://doi.org/10.1161/01.CIR.96.9.2920>
- Frangogiannis, N. G. (2006). The Mechanistic Basis of Infarct Healing. *Antioxidants*, 8, 1907–1939.
- Frangogiannis, N. G. (2014). The inflammatory response in myocardial injury, repair, and remodelling. *Nature Reviews Cardiology*, 11(5), 255–265. <https://doi.org/10.1038/nrcardio.2014.28>
- Frangogiannis, N. G. (2019). Cardiac fibrosis: Cell biological mechanisms, molecular pathways and therapeutic opportunities. *Molecular Aspects of Medicine*, 65(August 2018), 70–99. <https://doi.org/10.1016/j.mam.2018.07.001>
- Fukushima, K., Bravo, P. E., Higuchi, T., Karl, H., Dannals, R. F., Lardo, A. C., & Szabo, Z. (2013). *Molecular PET/CT Imaging of Cardiac Angiotensin II Type 1 Receptors*. 60(24), 2527–2534. <https://doi.org/10.1016/j.jacc.2012.09.023>
- Gao, H., Lang, L., Guo, N., Cao, F., Quan, Q., Hu, S., Kiesewetter, D. O., Niu, G., & Chen, X. (2012). PET imaging of angiogenesis after myocardial infarction/reperfusion using a one-step labeled integrin-targeted tracer 18F-AIF-NOTA-PRGD2. *European Journal of Nuclear Medicine and Molecular Imaging*, 39(4), 683–692. <https://doi.org/10.1007/s00259-011-2052-1>
- Gerber, B. L., Melin, J. A., Bol, A., Labar, D., Cogneau, M., Michel, C., & Vanoverschelde, J. L. (1998). Nitrogen-13-ammonia and oxygen-15-water estimates of absolute myocardial perfusion in

- left ventricular ischemic dysfunction. *Journal of Nuclear Medicine : Official Publication, Society of Nuclear Medicine*, 39(10), 1655–1662. <http://www.ncbi.nlm.nih.gov/pubmed/9776263>
- Gewirtz, H., & Dilsizian, V. (2017). Myocardial viability: survival mechanisms and molecular imaging targets in acute and chronic ischemia. *Circulation Research*, 120(7), 1197–1212. <https://doi.org/10.1161/CIRCRESAHA.116.307898>
- Gibson, M. S., Domingues, N., & Vieira, O. V. (2018). Lipid and Non-lipid Factors Affecting Macrophage Dysfunction and Inflammation in Atherosclerosis. *Frontiers in Physiology*, 9, 654. <https://doi.org/10.3389/fphys.2018.00654>
- Gnesin, S., Mitsakis, P., Cicone, F., Deshayes, E., Dunet, V., Gallino, A. F., Kosinski, M., Baechler, S., Buchegger, F., Viertl, D., & Prior, J. O. (2017). First in-human radiation dosimetry of 68Ga-NODAGA-RGDyK. *EJNMMI Research*, 7. <https://doi.org/10.1186/s13550-017-0288-x>
- Grassi, I., Nanni, C., Allegri, V., Morigi, J. J., Montini, G. C., Castellucci, P., & Fanti, S. (2012). The clinical use of PET with 11C-acetate. *American Journal of Nuclear Medicine and Molecular Imaging*, 2(1), 33–47. <http://www.pubmedcentral.nih.gov/articlerender.fcgi?artid=3478117&tool=pmcentrez&rendertype=abstract>
- Gupta, Mi., Vavasis, C., & Frishman, W. (2012). Heat shock proteins in cardiovascular diseases. *Heat Shock Proteins in Cardiovascular Diseases*, 12(1), 1–84. <https://doi.org/10.1097/01.crd.0000090894.70619.fa>
- Harms, H. J., de Haan, S., Knaapen, P., Allaart, C. P., Lammertsma, A. A., & Lubberink, M. (2011). Parametric images of myocardial viability using a single 15O-H<sub>2</sub>O PET/CT scan. *Journal of Nuclear Medicine : Official Publication, Society of Nuclear Medicine*, 52(5), 745–749. <https://doi.org/10.2967/jnumed.110.085431>
- Harms, H. J., Nesterov, S. V., Han, C., Danad, I., Leonora, R., Rajmakers, P. G., Lammertsma, A. A., Knuuti, J., & Knaapen, P. (2014). Comparison of clinical non-commercial tools for automated quantification of myocardial blood flow using oxygen-15-labelled water PET/CT. *European Heart Journal - Cardiovascular Imaging*, 15(4), 431–441. <https://doi.org/10.1093/ehjci/jet177>
- Hartikainen, J., Hassinen, I., Hedman, A., Kivelä, A., Saraste, A., Knuuti, J., Husso, M., Mussalo, H., Hedman, M., Rissanen, T. T., Toivanen, P., Heikura, T., Witztum, J. L., Tsimikas, S., & Ylä-Herttuala, S. (2017). Adenoviral intramyocardial VEGF-DDNDC gene transfer increases myocardial perfusion reserve in refractory angina patients: A phase I/IIa study with 1-year follow-up. *European Heart Journal*, 38(33), 2547–2555. <https://doi.org/10.1093/eurheartj/ehx352>
- Hartupee, J., & Mann, D. L. (2016). Neurohormonal activation in heart failure with reduced ejection fraction. *Nature Reviews Cardiology*, 14(1), 30–38. <https://doi.org/10.1038/nrcardio.2016.163>
- Hearse, D. J. (2000). The elusive coypu: The importance of collateral flow and the search for an alternative to the dog. *Cardiovascular Research*, 45(1), 215–219. [https://doi.org/10.1016/S0008-6363\(99\)00331-4](https://doi.org/10.1016/S0008-6363(99)00331-4)
- Henzlova, M. J., Duvall, W. L., Einstein, A. J., Travin, M. I., & Verberne, H. J. (2016). ASNC imaging guidelines for SPECT nuclear cardiology procedures: Stress, protocols, and tracers. *Journal of Nuclear Cardiology*, 23(3), 606–639. <https://doi.org/10.1007/s12350-015-0387-x>
- Herrero, P., Staudenherz, a, Walsh, J. F., Gropler, R. J., & Bergmann, S. R. (1995). Heterogeneity of myocardial perfusion provides the physiological basis of perfusable tissue index. *Journal of Nuclear Medicine : Official Publication, Society of Nuclear Medicine*, 36(2), 320–327. <http://www.ncbi.nlm.nih.gov/pubmed/7830138>
- Higuchi, T., Bengel, F. M., Seidl, S., Watzlowik, P., Kessler, H., Hegenloh, R., Reder, S., Nekolla, S. G., Wester, H. J., & Schwaiger, M. (2008). Assessment of alphavbeta3 integrin expression after myocardial infarction by positron emission tomography. *Cardiovascular Research*, 78(2), 395–403. <https://doi.org/10.1093/cvr/cvn033>
- Hinz, B. (2006). Masters and servants of the force: The role of matrix adhesions in myofibroblast force perception and transmission. *European Journal of Cell Biology*, 85(3–4), 175–181. <https://doi.org/10.1016/j.ejcb.2005.09.004>

- Horekmans, M., Ring, L., Duchene, J., Santovito, D., Schloss, M. J., Drechsler, M., Weber, C., Soehnlein, O., & Steffens, S. (2017). Neutrophils orchestrate post-myocardial infarction healing by polarizing macrophages towards a reparative phenotype. *European Heart Journal*, *38*(3), 187–197. <https://doi.org/10.1093/eurheartj/ehw002>
- Horstick, G., Bierbach, B., Abegunewardene, N., Both, S., Kuhn, S., Manefeld, D., Reinecke, H.-J., Vosseler, M., Helisch, A., Becker, D., Lauterbach, M., Kempfski, O., & Lehr, H.-A. (2009). Critical Single Proximal Left Arterial Descending Coronary Artery Stenosis to Mimic Chronic Myocardial Ischemia: A New Model Induced by Minimal Invasive Technology. *Journal of Vascular Research*, *46*(4), 290–298. <https://doi.org/10.1159/000181545>
- Hughes, G. C., Post, M. J., Simons, M., & Annex, B. H. (2003). Translational physiology: porcine models of human coronary artery disease: implications for preclinical trials of therapeutic angiogenesis. *Journal of Applied Physiology (Bethesda, Md. : 1985)*, *94*(5), 1689–1701. <https://doi.org/10.1152/jappphysiol.00465.2002>
- Huttala, O., Vuorenpää, H., Toimela, T., Uotila, J., Kuokkanen, H., Ylikomi, T., Sarkanen, J.-R., & Heinonen, T. (2015). Human vascular model with defined stimulation medium – a characterization study. *ALTEX*, *32*(2), 125–136. <https://doi.org/10.14573/altex.1411271>
- Hynes, R. O. (2002). Integrins: Bidirectional, allosteric signaling machines. *Cell*, *110*(6), 673–687. [https://doi.org/10.1016/S0092-8674\(02\)00971-6](https://doi.org/10.1016/S0092-8674(02)00971-6)
- Iida, H., Kanno, I., Takahashi, A., Miura, S., Murakami, M., Takahashi, K., Ono, Y., Shishido, F., Inugami, A., & Tomura, N. (1988). Measurement of absolute myocardial blood flow with H215O and dynamic positron-emission tomography. Strategy for quantification in relation to the partial-volume effect. *Circulation*, *78*(1), 104–115. <https://doi.org/10.1161/01.CIR.78.1.104>
- Iida, H., Rhodes, C., de Silva, R., Yamamoto, Y., Araujo, L., Maseri, A., & Jones, T. (1991). Myocardial tissue fraction--correction for partial volume effects and measure of tissue viability. *Journal of Nuclear Medicine : Official Publication, Society of Nuclear Medicine*, *32*(11), 2169–2175. <http://www.ncbi.nlm.nih.gov/pubmed/1941156>
- Iida, H., Rhodes, C. G., de Silva, R., Araujo, L. I., Bloomfield, P. M., Lammertsma, A. A., & Jones, T. (1992). Use of the left ventricular time-activity curve as a noninvasive input function in dynamic oxygen-15-water positron emission tomography. *Journal of Nuclear Medicine : Official Publication, Society of Nuclear Medicine*, *33*(9), 1669–1677. <http://www.ncbi.nlm.nih.gov/pubmed/1517842>
- Iida, H., Ruotsalainen, U., Mäki, M., Haaparnata, M., Bergman, J., Voipio-Pulkki, L. M., Nuutila, P., Koshino, K., & Knuuti, J. (2012). F-18 fluorodeoxyglucose uptake and water-perfusible tissue fraction in assessment of myocardial viability. *Annals of Nuclear Medicine*, *26*(8), 644–655. <https://doi.org/10.1007/s12149-012-0631-2>
- Iida, H., Takahashi, A., Tamura, Y., Ono, Y., & Lammertsma, a a. (1995). Myocardial blood flow: comparison of oxygen-15-water bolus injection, slow infusion and oxygen-15-carbon dioxide slow inhalation. *Journal of Nuclear Medicine : Official Publication, Society of Nuclear Medicine*, *36*(1), 78–85. <http://www.ncbi.nlm.nih.gov/pubmed/7799088>
- Iida, H., Tamura, Y., Kitamura, K., Bloomfield, P. M., Eberl, S., & Ono, Y. (2000). Histochemical correlates of (15)O-water-perfusible tissue fraction in experimental canine studies of old myocardial infarction. *Journal of Nuclear Medicine*, *41*(10), 1737–1745. <http://www.ncbi.nlm.nih.gov/pubmed/11038006>
- Itoh, H., Namura, M., Seki, H., Asai, T., Tsuchiya, T., Uenishi, H., Fujii, H., Fujita, S., Tanabe, Y., Ito, J., Shimizu, M., & Mabuchi, H. (2002). Perfusable tissue index obtained by positron emission tomography as a marker of myocardial viability in patients with ischemic ventricular dysfunction. *Circulation Journal*, *66*(4), 341–344. <https://doi.org/10.1253/circj.66.341>
- Jenkins, W. S. A., Vesey, A. T., Stirrat, C., Connell, M., Lucatelli, C., Neale, A., Moles, C., Vickers, A., Fletcher, A., Pawade, T., Wilson, I., Rudd, J. H. F., van Beek, E. J. R., Mirsadraee, S., Dweck, M. R., & Newby, D. E. (2016). Cardiac  $\alpha v \beta 3$  integrin expression following acute myocardial infarction in humans. *Heart*, *heartjnl-2016-310115*. <https://doi.org/10.1136/heartjnl-2016-310115>

- Johansson, I., Dahlström, U., Edner, M., Näsman, P., Rydén, L., & Norhammar, A. (2016). Prognostic Implications of Type 2 Diabetes Mellitus in Ischemic and Nonischemic Heart Failure. *Journal of the American College of Cardiology*, *68*(13), 1404–1416. <https://doi.org/10.1016/j.jacc.2016.06.061>
- Johnson, L. L., Schofield, L., Donahay, T., Bouchard, M., Poppas, A., & Haubner, R. (2008). Radiolabeled arginine-glycine-aspartic acid peptides to image angiogenesis in swine model of hibernating myocardium. *JACC. Cardiovascular Imaging*, *1*(4), 500–510. <https://doi.org/10.1016/j.jcmg.2008.05.002>
- Kaandorp, T. A. M., Lamb, H. J., Van Der Wall, E. E., de Roos, A., & Bax, J. J. (2005). Cardiovascular MR to assess myocardial viability in chronic ischaemic LV dysfunction. *Heart*, *91*(10), 1359–1365. <https://doi.org/10.1136/hrt.2003.025353>
- Kajander, S. a, Joutsiniemi, E., Saraste, M., Pietilä, M., Ukkonen, H., Saraste, A., Sipilä, H. T., Teräs, M., Mäki, M., Airaksinen, J., Hartiala, J., & Knuuti, J. (2011). Clinical value of absolute quantification of myocardial perfusion with (15)O-water in coronary artery disease. *Circulation. Cardiovascular Imaging*, *4*(6), 678–684. <https://doi.org/10.1161/CIRCIMAGING.110.960732>
- Kalinowski, L., Dobrucki, L. W., Meoli, D. F., Dione, D. P., Sadeghi, M. M., Madri, J. A., & Sinusas, A. J. (2008). Targeted imaging of hypoxia-induced integrin activation in myocardium early after infarction. *Journal of Applied Physiology (Bethesda, Md. : 1985)*, *104*(5), 1504–1512. <https://doi.org/10.1152/jappphysiol.00861.2007>
- Kaniscak, O., Khalil, H., Ivey, M. J., Karch, J., Maliken, B. D., Correll, R. N., Brody, M. J., Lin, S. C. J., Aronow, B. J., Tallquist, M. D., & Molkentin, J. D. (2016). Genetic lineage tracing defines myofibroblast origin and function in the injured heart. *Nature Communications*, *7*, 1–14. <https://doi.org/10.1038/ncomms12260>
- Kapp, T. G., Rechenmacher, F., Neubauer, S., Maltsev, O. V., Cavalcanti-Adam, E. A., Zarka, R., Reuning, U., Notni, J., Wester, H. J., Mas-Moruno, C., Spatz, J., Geiger, B., & Kessler, H. (2017). A comprehensive evaluation of the activity and selectivity profile of ligands for RGD-binding integrins. *Scientific Reports*, *7*(November 2016), 1–13. <https://doi.org/10.1038/srep39805>
- Kim, C., Ye, F., & Ginsberg, M. H. (2011). Regulation of Integrin Activation. *Annual Review of Cell and Developmental Biology*, *27*(1), 321–345. <https://doi.org/10.1146/annurev-cellbio-100109-104104>
- Kiugel, M., Dijkgraaf, I., Kytö, V., Helin, S., Liljenbäck, H., Saanijoki, T., Yim, C.-B., Oikonen, V., Saukko, P., Knuuti, J., Roivainen, A., & Saraste, A. (2014). Dimeric [(68)Ga]DOTA-RGD peptide targeting  $\alpha v \beta 3$  integrin reveals extracellular matrix alterations after myocardial infarction. *Molecular Imaging and Biology: MIB: The Official Publication of the Academy of Molecular Imaging*, *16*(6), 793–801. <https://doi.org/10.1007/s11307-014-0752-1>
- Klein, L. J., Visser, F. C., Knaapen, P., Peters, J. H., Teule, G. J. J., Visser, C. A., & Lammertsma, A. A. (2001). Carbon-11 acetate as a tracer of myocardial oxygen consumption. *European Journal of Nuclear Medicine*, *28*(5), 651–668. <https://doi.org/10.1007/s002590000472>
- Knaapen, P., Boellaard, R., Götte, M. J. W., van der Weerd, A. P., Visser, C. A., Lammertsma, A. A., & Visser, F. C. (2003). The perfusable tissue index: A marker of myocardial viability. *Journal of Nuclear Cardiology*, *10*(6), 684–691. [https://doi.org/10.1016/S1071-3581\(03\)00656-1](https://doi.org/10.1016/S1071-3581(03)00656-1)
- Knaapen, P., Bondarenko, O., Beek, A. M., Götte, M. J. W., Boellaard, R., van Weerd, A. P., Visser, C. A., van Rossum, A. C., Lammertsma, A. A., & Visser, F. C. (2006). Impact of scar on water-perfusable tissue index in chronic ischemic heart disease: Evaluation with PET and contrast-enhanced MRI. *Molecular Imaging and Biology*, *8*(4), 245–251. <https://doi.org/10.1007/s11307-006-0044-5>
- Knetsch, P. a, Petrik, M., Griessinger, C. M., Rangger, C., Fani, M., Kesenheimer, C., von Guggenberg, E., Pichler, B. J., Virgolini, I., Decristoforo, C., & Haubner, R. (2011). [68Ga]NODAGA-RGD for imaging  $\alpha v \beta 3$  integrin expression. *European Journal of Nuclear Medicine and Molecular Imaging*, *38*(7), 1303–1312. <https://doi.org/10.1007/s00259-011-1778-0>

- Knuuti, J., Kajander, S., Mäki, M., & Ukkonen, H. (2009). Quantification of myocardial blood flow will reform the detection of CAD. *Journal of Nuclear Cardiology*, *16*(4), 497–506. <https://doi.org/10.1007/s12350-009-9101-1>
- Knuuti, J., Wijns, W., Saraste, A., Capodanno, D., Barbato, E., Funck-Brentano, C., Prescott, E., Storey, R. F., Deaton, C., Cuisset, T., Agewall, S., Dickstein, K., Edvardsen, T., Escaned, J., Gersh, B. J., Svitil, P., Gilard, M., Hasdai, D., Hatala, R., ... Bax, J. J. (2020). 2019 ESC guidelines for the diagnosis and management of chronic coronary syndromes. *European Heart Journal*, *41*(3), 407–477. <https://doi.org/10.1093/eurheartj/ehz425>
- Kobayashi, K., Maeda, K., Takefuji, M., Kikuchi, R., Morishita, Y., Hirashima, M., & Murohara, T. (2017). Dynamics of angiogenesis in ischemic areas of the infarcted heart. *Scientific Reports*, *7*(1), 1–13. <https://doi.org/10.1038/s41598-017-07524-x>
- Kolwicz, S. C., Purohit, S., & Tian, R. (2013). Cardiac metabolism and its interactions with contraction, growth, and survival of cardiomyocytes. *Circulation Research*, *113*(5), 603–616. <https://doi.org/10.1161/CIRCRESAHA.113.302095>
- Laitinen, I., Notni, J., Pohle, K., Rudelius, M., Farrell, E., Nekolla, S. G., Henriksen, G., Neubauer, S., Kessler, H., Wester, H.-J., & Schwaiger, M. (2013). Comparison of cyclic RGD peptides for  $\alpha v \beta 3$  integrin detection in a rat model of myocardial infarction. *EJNMMI Research*, *3*(1), 38. <https://doi.org/10.1186/2191-219X-3-38>
- Lapa, C., Reiter, T., Werner, R. A., Ertl, G., Wester, H.-J., Buck, A. K., Bauer, W. R., & Herrmann, K. (2015). *[68Ga]Pentixafor-PET/CT for Imaging of Chemokine Receptor 4 Expression After Myocardial Infarction*. *8*(12), 1465–1468.
- Lee, W. W., Marinelli, B., Laan, A. M. Van Der, Sena, B., Gorbato, R., Leuschner, F., Dutta, P., Iwamoto, Y., Ueno, T., Begieneman, M. P. V., Niessen, H. W. M., Piek, J. J., Vinegoni, C., Pittet, M. J., Swirski, F. K., Tawakol, A., Carli, M. Di, & Weissleder, R. (2012). *PET/MRI of inflammation in myocardial infarction*. *59*(2), 153–163. <https://doi.org/10.1016/j.jacc.2011.08.066>.PET/MRI
- Lelovas, P. P., Kostomitsopoulos, N. G., & Xanthos, T. T. (2014). A comparative anatomic and physiologic overview of the porcine heart. *Journal of the American Association for Laboratory Animal Science : JAALAS*, *53*(5), 432–438. <http://www.ncbi.nlm.nih.gov/pubmed/25255064>
- Libby, P. (2002). Inflammation in atherosclerosis. *Nature*, *420*(6917), 868–874. <https://doi.org/10.1038/nature01323>
- Liehn, E. A., Postea, O., Curaj, A., & Marx, N. (2011). Repair after myocardial infarction, between fantasy and reality: The role of chemokines. *Journal of the American College of Cardiology*, *58*(23), 2357–2362. <https://doi.org/10.1016/j.jacc.2011.08.034>
- Maddahi, J. (2012). Properties of an ideal PET perfusion tracer: New PET tracer cases and data. *Journal of Nuclear Cardiology*, *19*(SUPPL. 1), 30–37. <https://doi.org/10.1007/s12350-011-9491-8>
- Maddahi, J., & Packard, R. R. S. (2014). Cardiac PET perfusion tracers: current status and future directions. *Seminars in Nuclear Medicine*, *44*(5), 333–343. <https://doi.org/10.1053/j.semnuclmed.2014.06.011>
- Majno, G., & Joris, I. (1995). Apoptosis, Oncosis and Necrosis. An Overview of Cell Death. *American Journal of Pathology*, *146*(1), 3–15.
- Makowski, M. R., Ebersberger, U., Nekolla, S., & Schwaiger, M. (2008). In vivo molecular imaging of angiogenesis, targeting  $\alpha v \beta 3$  integrin expression, in a patient after acute myocardial infarction. *European Heart Journal*, *29*(18), 2201. <https://doi.org/10.1093/eurheartj/ehn129>
- Mandic, L., Traxler, D., Gugerell, A., Zlabinger, K., Lukovic, D., Pavo, N., Goliash, G., Spannbauer, A., Winkler, J., & Gyöngyösi, M. (2016). Molecular Imaging of Angiogenesis in Cardiac Regeneration. *Current Cardiovascular Imaging Reports*, *9*(10). <https://doi.org/10.1007/s12410-016-9389-6>
- Manso, A. M., Kang, S.-M., & Ross, R. S. (2009). Integrins, focal adhesions, and cardiac fibroblasts. *Journal of Investigative Medicine : The Official Publication of the American Federation for Clinical Research*, *57*(8), 856–860. <https://doi.org/10.231/JIM.0b013e3181c5e61f>

- McDiarmid, A. K., Pellicori, P., Cleland, J. G., & Plein, S. (2017). Taxonomy of segmental myocardial systolic dysfunction. *European Heart Journal*, *38*(13), 942–954. <https://doi.org/10.1093/eurheartj/ehw140>
- McMurray, J. J. V., & Pfeffer, M. A. (2004). Heart Failure. *The Lancet*, *365*, 1877–1889. <https://doi.org/10.1161/01.CIR.0000134279.79571.73>
- Mehran, R., Ricci, M., Graham, A., Carter, K., & Symes, J. (1991). Porcine Model for Vascular Graft Studies. *Journal of Investigative Surgery*, *4*, 37–44.
- Menichetti, L., Kusmic, C., Panetta, D., Arosio, D., Petroni, D., Matteucci, M., Salvadori, P. A., Casagrande, C., L'Abbate, A., & Manzoni, L. (2013). MicroPET/CT imaging of  $\alpha v \beta 3$  integrin via a novel  $^{68}\text{Ga}$ -NOTA-RGD peptidomimetic conjugate in rat myocardial infarction. *European Journal of Nuclear Medicine and Molecular Imaging*, *40*(8), 1265–1274. <https://doi.org/10.1007/s00259-013-2432-9>
- Meoli, D. F., Sadeghi, M. M., Krassilnikova, S., Bourke, B. N., Giordano, F. J., Dione, D. P., Su, H., Edwards, D. S., Liu, S., Harris, T. D., Madri, J. a., Zaret, B. L., & Sinusas, A. J. (2004). Noninvasive imaging of myocardial angiogenesis following experimental myocardial infarction. *Journal of Clinical Investigation*, *113*(12), 1684–1691. <https://doi.org/10.1172/JCI200420352>
- Moran, A. E., Forouzanfar, M. H., Roth, G. A., Mensah, G. A., Ezzati, M., Murray, C. J. L., & Naghavi, M. (2014). Temporal Trends in Ischemic Heart Disease Mortality in 21 World Regions, 1980 to 2010. *Circulation*, *129*(14), 1483–1492. <https://doi.org/10.1161/CIRCULATIONAHA.113.004042>
- Morooka, M., Kubota, K., Kadowaki, H., Ito, K., Okazaki, O., Kashida, M., Mitsumoto, T., Iwata, R., Ohtomo, K., & Hiroe, M. (2009).  $^{11}\text{C}$ -methionine PET of acute myocardial infarction. *Journal of Nuclear Medicine*, *50*(8), 1283–1287. <https://doi.org/10.2967/jnumed.108.061341>
- Murray, I. R., Gonzalez, Z. N., Baily, J., Dobie, R., Wallace, R. J., Mackinnon, A. C., Smith, J. R., Greenhalgh, S. N., Thompson, A. I., Conroy, K. P., Griggs, D. W., Ruminiski, P. G., Gray, G. A., Singh, M., Campbell, M. A., Kendall, T. J., Dai, J., Li, Y., Iredale, J. P., ... Henderson, N. C. (2017).  $\alpha v$  Integrins on Mesenchymal Cells Regulate Skeletal and Cardiac Muscle Fibrosis. *Nature Communications*, *8*(1). <https://doi.org/10.1038/s41467-017-01097-z>
- Muzik, O., Beanlands, R. S. B., Hutchins, G. D., Mangner, T. J., Nguyen, N., & Schwaiger, M. (1993). Validation of nitrogen-13-ammonia tracer kinetic model for quantification of myocardial blood flow using PET. *Journal of Nuclear Medicine*, *34*(1), 83–91.
- Nahrendorf, M., Swirski, F. K., Aikawa, E., Stangenberg, L., Wurdinger, T., Figueiredo, J.-L., Libby, P., Weissleder, R., & Pittet, M. J. (2007). The healing myocardium sequentially mobilizes two monocyte subsets with divergent and complementary functions. *The Journal of Experimental Medicine*, *204*(12), 3037–3047. <https://doi.org/10.1084/jem.20070885>
- Nowbar, A. N., Gitto, M., Howard, J. P., Francis, D. P., & Al-Lamee, R. (2019). Mortality From Ischemic Heart Disease. *Circulation Cardiovascular Quality and Outcomes*, *12*(6), e005375. <https://doi.org/10.1161/CIRCOUTCOMES.118.005375>
- Ono, K., Matsumori, A., Shioi, T., Furukawa, Y., & Sasayama, S. (1998). Cytokine gene expression after myocardial infarction in rat hearts: Possible implication in left ventricular remodeling. *Circulation*, *98*(2), 149–156. <https://doi.org/10.1161/01.CIR.98.2.149>
- Orbay, H., Zhang, Y., Valdovinos, H. F., Song, G., Hernandez, R., Theuer, C. P., Hacker, T. A., Nickles, R. J., & Cai, W. (2013). Positron emission tomography imaging of CD105 expression in a rat myocardial infarction model with  $^{64}\text{Cu}$ -NOTA-TRC105. *American Journal of Nuclear Medicine and Molecular Imaging*, *4*(1), 1–9. <http://www.ncbi.nlm.nih.gov/pubmed/24380040>
- Park, J. S., Svetkauskaite, D., He, Q., Kim, J. Y., Strassheim, D., Ishizaka, A., & Abraham, E. (2004). Involvement of Toll-like Receptors 2 and 4 in Cellular Activation by High Mobility Group Box 1 Protein. *Journal of Biological Chemistry*, *279*(9), 7370–7377. <https://doi.org/10.1074/jbc.M306793200>
- Patel, H., Mazur, W., Williams, K. A., & Kalra, D. K. (2018). Myocardial viability—State of the art: Is it still relevant and how to best assess it with imaging? *Trends in Cardiovascular Medicine*, *28*(1), 24–37. <https://doi.org/10.1016/j.tcm.2017.07.001>

- Pfeffer, M. A., & Braunwald, E. (1990). Ventricular remodeling after myocardial infarction. Experimental observations and clinical implications. *Circulation*, *81*(4), 1161–1172. <https://doi.org/10.1161/01.CIR.81.4.1161>
- Phelps, M. E. (2000). PET: The merging of biology and imaging into molecular imaging. *Journal of Nuclear Medicine*, *41*(4), 661–681.
- Ponikowski, P., Voors, A. A., Anker, S. D., Bueno, H., Cleland, J. G. F., Coats, A. J. S., Falk, V., González-Juanatey, J. R., Harjola, V.-P., Jankowska, E. A., Jessup, M., Linde, C., Nihoyannopoulos, P., Parissis, J. T., Pieske, B., Riley, J. P., Rosano, G. M. C., Ruilope, L. M., Ruschitzka, F., ... Davies, C. (2016). 2016 ESC Guidelines for the diagnosis and treatment of acute and chronic heart failure. *European Heart Journal*, *37*(27), 2129–2200. <https://doi.org/10.1093/eurheartj/ehw128>
- Prabhu, S. D., & Frangogiannis, N. G. (2016). The Biological Basis for Cardiac Repair After Myocardial Infarction: From Inflammation to Fibrosis. *Circulation Research*, *119*(1), 91–112. <https://doi.org/10.1161/CIRCRESAHA.116.303577>
- Rahimtoola, S. H. (1989). The Hibernating Myocardium: Implications for Management. *American Heart Journal*, *117*, 211–221.
- Rasmussen, T., Follin, B., Kastrup, J., Brandt-Larsen, M., Madsen, J., Emil Christensen, T., Pharo Hammelev, K., Hasbak, P., & Kjær, A. (2016a). Angiogenesis PET Tracer Uptake (68Ga-NODAGA-E[(cRGDyK)]<sub>2</sub>) in Induced Myocardial Infarction in Minipigs. *Diagnostics*, *6*(2), 26. <https://doi.org/10.3390/diagnostics6020026>
- Rasmussen, T., Follin, B., Kastrup, J., Christensen, T. E., Hammelev, K. P., Kjær, A., & Hasbak, P. (2016b). Myocardial perfusion of infarcted and normal myocardium in propofol-anesthetized minipigs using 82Rubidium PET. *Journal of Nuclear Cardiology*, *23*(3), 599–603. <https://doi.org/10.1007/s12350-016-0453-z>
- Razeghi, P., Young, M. E., Alcorn, J. L., Moravec, C. S., Frazier, O. H., & Taegtmeier, H. (2001). Metabolic gene expression in fetal and failing human heart. *Circulation*, *104*(24), 2923–2931. <https://doi.org/10.1161/hc4901.100526>
- Reimer, K. A., Lowe, J. E., Rasmussen, M. M., & Jennings, R. B. (1977). The wavefront phenomenon of ischemic cell death. 1. Myocardial infarct size vs duration of coronary occlusion in dogs. *Circulation*, *56*(5), 786–794. <https://doi.org/10.1161/01.CIR.56.5.786>
- Reinmuth, N., Liu, W., Ahmad, S. A., Fan, F., Stoeltzing, O., Parikh, A. A., Bucana, C. D., Gallick, G. E., Nickols, M. A., Westlin, W. F., & Ellis, L. M. (2003).  $\alpha v \beta 3$  integrin antagonist S247 decreases colon cancer metastasis and angiogenesis and improves survival in mice. *Cancer Research*, *63*(9), 2079–2087.
- Reiter, T., Kircher, M., Schirbel, A., Werner, R. A., Kropf, S., Ertl, G., Buck, A. K., Wester, H. J., Bauer, W. R., & Lapa, C. (2018). Imaging of C-X-C Motif Chemokine Receptor CXCR4 Expression After Myocardial Infarction With [ 68 Ga]Pentixafor-PET/CT in Correlation With Cardiac MRI. *JACC: Cardiovascular Imaging*, *11*(10), 1541–1543. <https://doi.org/10.1016/j.jcmg.2018.01.001>
- Rischpler, C., Dirschinger, R. J., Nekolla, S. G., Kossmann, H., Nicolosi, S., Hanus, F., van Marwick, S., Kunze, K. P., Meinicke, A., Götze, K., Kastrati, A., Langwieser, N., Ibrahim, T., Nahrendorf, M., Schwaiger, M., & Laugwitz, K.-L. (2016). Prospective Evaluation of 18F-Fdg Uptake in Post-Ischemic Myocardium By Simultaneous Pet/Mri As a Prognostic Marker of Functional Outcome. *Circulation. Cardiovascular Imaging*, *9*(4), e004316. <https://doi.org/10.1161/CIRCIMAGING.115.004316>
- Rissanen, T. T., Nurro, J., Halonen, P. J., Tarkia, M., Saraste, A., Rannankari, M., Honkonen, K., Pietilä, M., Leppänen, O., Kuivaniemi, A., Knuuti, J., & Ylä-Herttuala, S. (2013). The bottleneck stent model for chronic myocardial ischemia and heart failure in pigs. *American Journal of Physiology. Heart and Circulatory Physiology*, *305*(9), H1297–308. <https://doi.org/10.1152/ajpheart.00561.2013>

- Rosenkranz, S. (2004). TGF- $\beta$ 1 and angiotensin networking in cardiac remodeling. *Cardiovascular Research*, 63(3), 423–432. <https://doi.org/10.1016/j.cardiores.2004.04.030>
- Rossi, A., Uitterdijk, A., Dijkshoorn, M., Klotz, E., Dharampal, A., Van Straten, M., Van Der Giessen, W. J., Mollet, N., Van Geuns, R. J., Krestin, G. P., Duncker, D. J., De Feyter, P. J., & Merkus, D. (2013). Quantification of myocardial blood flow by adenosine-stress CT perfusion imaging in pigs during various degrees of stenosis correlates well with coronary artery blood flow and fractional flow reserve. *European Heart Journal Cardiovascular Imaging*, 14(4), 331–338. <https://doi.org/10.1093/ehjci/jcs150>
- Rotteveel, L., Poot, A. J., Bogaard, H. J., ten Dijke, P., Lammertsma, A. A., & Windhorst, A. D. (2019). In vivo imaging of TGF $\beta$  signalling components using positron emission tomography. *Drug Discovery Today*. <https://doi.org/10.1016/j.drudis.2019.08.011>
- Ruoslahti, E., & Pierschbacher, M. D. (1987). New perspectives in cell adhesion: RGD and integrins. *Science*, 238(4826), 491–497. <https://doi.org/10.1126/science.2821619>
- Ryan, M. J., & Perera, D. (2018). Identifying and Managing Hibernating Myocardium: What’s New and What Remains Unknown? *Current Heart Failure Reports*, 15(4), 214–223. <https://doi.org/10.1007/s11897-018-0396-6>
- Saab, R., & Hage, F. G. (2017). Vasodilator stress agents for myocardial perfusion imaging. *Journal of Nuclear Cardiology*, 24(2), 434–438. <https://doi.org/10.1007/s12350-016-0408-4>
- Saraste, A., Kajander, S., Han, C., Nesterov, S. V., & Knuuti, J. (2012). PET: Is myocardial flow quantification a clinical reality? *Journal of Nuclear Cardiology*, 19(5), 1044–1059. <https://doi.org/10.1007/s12350-012-9588-8>
- Saraste, A., & Knuuti, J. (2017). PET imaging in heart failure: the role of new tracers. *Heart Failure Reviews*, 22(4), 501–511. <https://doi.org/10.1007/s10741-017-9620-9>
- Sarkanen, J. R., Mannerström, M., Vuorenää, H., Uotila, J., Ylikomi, T., & Heinonen, T. (2011). Intra-laboratory pre-validation of a human cell based in vitro angiogenesis assay for testing angiogenesis modulators. *Frontiers in Pharmacology*, JAN(January), 1–13. <https://doi.org/10.3389/fphar.2010.00147>
- Sarrazy, V., Koehler, A., Chow, M. L., Zimina, E., Li, C. X., Kato, H., Caldarone, C. A., & Hinz, B. (2014). Integrins  $\alpha$ v $\beta$ 5 and  $\alpha$ v $\beta$ 3 promote latent TGF- $\beta$ 1 activation by human cardiac fibroblast contraction. *Cardiovascular Research*, 102(3), 407–417. <https://doi.org/10.1093/cvr/cvu053>
- Schelbert, H. R., Phelps, M. E., Huang, S. C., MacDonald, N. S., Hansen, H., Selin, C., & Kuhl, D. E. (1981). N-13 ammonia as an indicator of myocardial blood flow. *Circulation*, 63(6 I), 1259–1272. <https://doi.org/10.1161/01.CIR.63.6.1259>
- Schinkel, A. F. L., Bax, J. J., Poldermans, D., Elhendy, A., Ferrari, R., & Rahimtoola, S. H. (2007). Hibernating Myocardium: Diagnosis and Patient Outcomes. *Current Problems in Cardiology*, 32(7), 375–410. <https://doi.org/10.1016/J.CPCARDIOL.2007.04.001>
- Schinkel, A. F. L., Poldermans, D., Vanoverschelde, J. L. J., Elhendy, A., Boersma, E., Roelandt, J. R. T. C., & Bax, J. J. (2004). Incidence of recovery of contractile function following revascularization in patients with ischemic left ventricular dysfunction. *American Journal of Cardiology*, 93(1), 14–17. <https://doi.org/10.1016/j.amjcard.2003.09.005>
- Schwarz, E. R., Schoendube, F. A., Kostin, S., Schmiedtke, N., Schulz, G., Buell, U., Messmer, B. J., Morrison, J., Hanrath, P., & vom Dahl, J. (1998). Prolonged Myocardial Hibernation Exacerbates Cardiomyocyte Degeneration and Impairs Recovery of Function After Revascularization. *Journal of the American College of Cardiology*, 31(5), 1018–1026. [https://doi.org/10.1016/S0735-1097\(98\)00041-2](https://doi.org/10.1016/S0735-1097(98)00041-2)
- Senior, R., & Lahiri, A. (1995). Enhanced detection of myocardial ischemia by stress dobutamine echocardiography utilizing the “biphasic” response of wall thickening during low and high dose dobutamine infusion. *Journal of the American College of Cardiology*, 26(1), 26–32. [https://doi.org/10.1016/0735-1097\(95\)00139-Q](https://doi.org/10.1016/0735-1097(95)00139-Q)
- Sherif, H. M., Saraste, A., Nekolla, S. G., Weidl, E., Reder, S., Tapfer, A., Rudelius, M., Higuchi, T., Botnar, R. M., Wester, H.-J., & Schwaiger, M. (2012). Molecular imaging of early  $\alpha$ v $\beta$ 3 integrin



- expression predicts long-term left-ventricle remodeling after myocardial infarction in rats. *Journal of Nuclear Medicine: Official Publication, Society of Nuclear Medicine*, 53(2), 318–323. <https://doi.org/10.2967/jnumed.111.091652>
- Soehnlein, O., & Lindbom, L. (2010). Phagocyte partnership during the onset and resolution of inflammation. *Nature Reviews Immunology*, 10(6), 427–439. <https://doi.org/10.1038/nri2779>
- Stanley, W. C., Recchia, F. A., & Lopaschuk, G. D. (2005). Myocardial Substrate Metabolism in the Normal and Failing Heart. *Physiological Reviews*, 85(3), 1093–1129. <https://doi.org/10.1152/physrev.00006.2004>
- Stary, H., Chandler, A., Glagov, S., Jr, G., Insull, W., Rosenfeld, M. J., Schaffer, S., Schwartz, C., Wagner, W., & Wissler, R. (1994). AHA Medical / Scientific Statement Special Report A Definition of Initial, Fatty Streak, and Intermediate Lesions of Atherosclerosis. *Circulation*, 89, 2462–2478. <https://doi.org/10.1161/01.CIR.89.5.2462>
- Sun, Opavsky, M. A., Stewart, D. J., Rabinovitch, M., Dawood, F., Wen, W. H., & Liu, P. P. (2003). Temporal response and localization of integrins  $\beta 1$  and  $\beta 3$  in the heart after myocardial infarction: Regulation by cytokines. *Circulation*, 107(7), 1046–1052. <https://doi.org/10.1161/01.CIR.0000051363.86009.3C>
- Sun, Zeng, Y., Zhu, Y., Feng, F., Xu, W., Wu, C., Xing, B., Zhang, W., Wu, P., Cui, L., Wang, R., Li, F., Chen, X., & Zhu, Z. (2014). Application of (68)Ga-PRGD2 PET/CT for  $\alpha\beta 3$ -integrin imaging of myocardial infarction and stroke. *Theranostics*, 4(8), 778–786. <https://doi.org/10.7150/thno.8809>
- Swindle, M. M., Makin, A., Herron, A. J., Clubb, F. J., & Frazier, K. S. (2012). Swine as Models in Biomedical Research and Toxicology Testing. *Veterinary Pathology*, 49(2), 344–356. <https://doi.org/10.1177/0300985811402846>
- Taegt Mayer, H., Sen, S., & Vela, D. (2010). Return to the fetal gene program. *Ann NY Acad Sci*, 1188, 191–198. <https://doi.org/10.1038/jid.2014.371>
- Takagi, J., Petre, B. M., Walz, T., & Springer, T. A. (2002). Global conformational rearrangements in integrin extracellular domains in outside-in and inside-out signaling. *Cell*, 110(5), 599–611. [https://doi.org/10.1016/S0092-8674\(02\)00935-2](https://doi.org/10.1016/S0092-8674(02)00935-2)
- Tarkia, M., Saraste, A., Saanijoki, T., Oikonen, V., Vähäsilta, T., Strandberg, M., Stark, C., Tolvanen, T., Teräs, M., Savunen, T., Green, M. A., Knuuti, J., & Roivainen, A. (2012). Evaluation of 68Ga-labeled tracers for PET imaging of myocardial perfusion in pigs. *Nuclear Medicine and Biology*, 39(5), 715–723. <https://doi.org/10.1016/j.nucmedbio.2011.11.007>
- Tarkia, M., Stark, C., Haavisto, M., Kentala, R., Vähäsilta, T., Savunen, T., Strandberg, M., Hynninen, V. V., Saunavaara, V., Tolvanen, T., Teräs, M., Rokka, J., Pietilä, M., Saukko, P., Roivainen, A., Saraste, A., & Knuuti, J. (2015). Cardiac remodeling in a new pig model of chronic heart failure: Assessment of left ventricular functional, metabolic, and structural changes using PET, CT, and echocardiography. *Journal of Nuclear Cardiology*, 655–665. <https://doi.org/10.1007/s12350-015-0068-9>
- Teramoto, N., Koshino, K., Yokoyama, I., Miyagawa, S., Zeniya, T., Hirano, Y., Fukuda, H., Enmi, J., Sawa, Y., Knuuti, J., & Iida, H. (2011). Experimental pig model of old myocardial infarction with long survival leading to chronic left ventricular dysfunction and remodeling as evaluated by PET. *Journal of Nuclear Medicine: Official Publication, Society of Nuclear Medicine*, 52(5), 761–768. <https://doi.org/10.2967/jnumed.110.084848>
- Thackeray, Bankstahl, J. P., Wang, Y., Wollert, K. C., & Bengel, F. M. (2016). Targeting amino acid metabolism for molecular imaging of inflammation early after myocardial infarction. *Theranostics*, 6(11), 1768–1779. <https://doi.org/10.7150/thno.15929>
- Thackeray, Derlin, T., Haghikia, A., Napp, L. C., Wang, Y., Ross, T. L., Schäfer, A., Tillmanns, J., Wester, H. J., Wollert, K. C., Bauersachs, J., & Bengel, F. M. (2015). Molecular Imaging of the Chemokine Receptor CXCR4 after Acute Myocardial Infarction. *JACC: Cardiovascular Imaging*, 8(12), 1417–1426. <https://doi.org/10.1016/j.jcmg.2015.09.008>

- Thackeray, J., Hupe, H., Wang, Y., Bankstahl, J., Berding, G., Ross, T. L., Bauersachs, J., Wollert, K. C., & Bengel, F. M. (2018). Myocardial Inflammation Predicts Remodeling and Neuroinflammation After Myocardial Infarction. *JACC*, *71*(3), 263–267.
- Thygesen, K., Alpert, J. S., Jaffe, A. S., Chaitman, B. R., Bax, J. J., Morrow, D. A., White, H. D., Thygesen, K., Alpert, J. S., Jaffe, A. S., Chaitman, B. R., Bax, J. J., Morrow, D. A., White, H. D., Mickley, H., Crea, F., Van de Werf, F., Bucciarelli-Ducci, C., Katus, H. A., ... Corbett, S. (2019). Fourth universal definition of myocardial infarction (2018). *European Heart Journal*, *40*(3), 237–269. <https://doi.org/10.1093/eurheartj/ehy462>
- Tillisch, J., Brunken, R., Marshall, R., Schwaiger, M., Mandelkern, M., Phelps, M., & Schelbert, H. (1986). Reversibility of Cardiac Wall-Motion Abnormalities Predicted by Positron Tomography. *New England Journal of Medicine*, *314*(14), 884–888. <https://doi.org/10.1056/NEJM198604033141405>
- Timmer, S. A. J., Teunissen, P. F. A., Danad, I., Robbers, L. F. H. J., Raijmakers, P. G. H. M., Nijveldt, R., van Rossum, A. C., Lammertsma, A. A., van Royen, N., & Knaapen, P. (2017). In vivo assessment of myocardial viability after acute myocardial infarction: A head-to-head comparison of the perfusable tissue index by PET and delayed contrast-enhanced CMR. *Journal of Nuclear Cardiology*, *24*(2), 657–667. <https://doi.org/10.1007/s12350-015-0329-7>
- Toimela, T., Huttala, O., Sabell, E., Mannerström, M., Sarkanen, J. R., Ylikomi, T., & Heinonen, T. (2017). Intra-laboratory validated human cell-based in vitro vasculogenesis/angiogenesis test with serum-free medium. *Reproductive Toxicology*, *70*, 116–125. <https://doi.org/10.1016/j.reprotox.2016.11.015>
- Travers, J. G., Kamal, F. A., Robbins, J., Yutzey, K. E., & Blaxall, B. C. (2016). Cardiac fibrosis. *Circulation Research*, *118*(6), 1021–1040. <https://doi.org/10.1161/circresaha.115.306565>
- Turner, N. a, & Porter, K. E. (2013). Function and fate of myofibroblasts after myocardial infarction. *Fibrogenesis & Tissue Repair*, *6*(1), 5. <https://doi.org/10.1186/1755-1536-6-5>
- Tweet, M. S., Arruda-Olson, A. M., Anavekar, N. S., & Pellikka, P. A. (2015). Stress Echocardiography: What Is New and How Does It Compare with Myocardial Perfusion Imaging and Other Modalities? *Current Cardiology Reports*, *17*(6), 43. <https://doi.org/10.1007/s11886-015-0600-1>
- van den Borne, S. W. M., Diez, J., Blankesteijn, W. M., Verjans, J., Hofstra, L., & Narula, J. (2009). Myocardial remodeling after infarction: the role of myofibroblasts. *Nature Reviews Cardiology*, *7*(1), 30–37. <https://doi.org/10.1038/nrcardio.2009.199>
- van den Borne, S. W. M., Isobe, S., Verjans, J. W., Petrov, A., Lovhaug, D., Li, P., Zandbergen, H. R., Ni, Y., Frederik, P., Zhou, J., Arbo, B., Rogstad, A., Cuthbertson, A., Chettibi, S., Reutelingsperger, C., Blankesteijn, W. M., Smits, J. F. M., Daemen, M. J. A. P., Zannad, F., ... Narula, J. (2008). Molecular imaging of interstitial alterations in remodeling myocardium after myocardial infarction. *Journal of the American College of Cardiology*, *52*(24), 2017–2028. <https://doi.org/10.1016/j.jacc.2008.07.067>
- Van Der Gucht, A., Pomoni, A., Jreige, M., Allemann, P., & Prior, J. O. (2016). 68Ga-NODAGA-RGDyK PET/CT Imaging in Esophageal Cancer. *Clinical Nuclear Medicine*, *00*(00), 1. <https://doi.org/10.1097/RLU.0000000000001365>
- Von Degenfeld, G., Raake, P., Kupatt, C., Lebherz, C., Hinkel, R., Gildehaus, F. J., Münzing, W., Kranz, A., Waltenberger, J., Simoes, M., Schwaiger, M., Thein, E., & Boekstegers, P. (2003). Selective pressure-regulated retroinfusion of fibroblast growth factor-2 into the coronary vein enhances regional myocardial blood flow and function in pigs with chronic myocardial ischemia. *Journal of the American College of Cardiology*, *42*(6), 1120–1128. [https://doi.org/10.1016/S0735-1097\(03\)00915-X](https://doi.org/10.1016/S0735-1097(03)00915-X)
- Wadsak, W., & Mitterhauser, M. (2010). Basics and principles of radiopharmaceuticals for PET/CT. *European Journal of Radiology*, *73*(3), 461–469. <https://doi.org/10.1016/J.EJRAD.2009.12.022>
- Westman, P. C., Lipinski, M. J., Luger, D., Waksman, R., Bonow, R. O., Wu, E., & Epstein, S. E. (2016). Inflammation as a Driver of Adverse Left Ventricular Remodeling after Acute Myocardial

- Infarction. *Journal of the American College of Cardiology*, 67(17), 2050–2060. <https://doi.org/10.1016/j.jacc.2016.01.073>
- Wijns, W., Vatner, S. F., & Camici, P. G. (1998). Hibernating Myocardium. *New England Journal of Medicine*, 339(3), 173–181. <https://doi.org/10.1056/NEJM199807163390307>
- Windecker, S., Kolh, P., Alfonso, F., Collet, J.-P., Cremer, J., Falk, V., Filippatos, G., Hamm, C., Head, S. J., Jüni, P., Kappetein, A. P., Kastrati, A., Knuuti, J., Landmesser, U., Laufer, G., Neumann, F.-J., Richter, D. J., Schauerte, P., Uva, M. S., ... Davies, J. (2014). 2014 ESC/EACTS Guidelines on myocardial revascularization. *European Heart Journal*, 35(37), 2541–2619. <https://doi.org/10.1093/eurheartj/ehu278>
- Wu, Bogaert, J., D’hooge, J., Sipido, K., Maes, F., Dymarkowski, S., Rademakers, F. E., & Claus, P. (2010). Closed-chest animal model of chronic coronary artery stenosis. Assessment with magnetic resonance imaging. *The International Journal of Cardiovascular Imaging*, 26(3), 299–308. <https://doi.org/10.1007/s10554-009-9551-1>
- Wu, E., Ortiz, J. T., Tejedor, P., Lee, D. C., Bucciarelli-Ducci, C., Kansal, P., Carr, J. C., Holly, T. A., Lloyd-Jones, D., Klocke, F. J., & Bonow, R. O. (2008). Infarct size by contrast enhanced cardiac magnetic resonance is a stronger predictor of outcomes than left ventricular ejection fraction or end-systolic volume index: Prospective cohort study. *Heart*, 94(6), 730–736. <https://doi.org/10.1136/hrt.2007.122622>
- Yalamanchili, P., Wexler, E., Hayes, M., Yu, M., Bozek, J., Kagan, M., Radeke, H. S., Azure, M., Purohit, A., Casebier, D. S., & Robinson, S. P. (2007). Mechanism of uptake and retention of F-18 BMS-747158-02 in cardiomyocytes: A novel PET myocardial imaging agent. *Journal of Nuclear Cardiology*, 14(6), 782–788. <https://doi.org/10.1016/j.nuclcard.2007.07.009>
- Yamamoto, Y., de Silva, R., Rhodes, C. G., Araujo, L. I., Iida, H., Rechavia, E., Nihoyannopoulos, P., Hackett, D., Galassi, A. R., & Taylor, C. J. (1992). A new strategy for the assessment of viable myocardium and regional myocardial blood flow using 15O-water and dynamic positron emission tomography. *Circulation*, 86(1), 167–178. <https://doi.org/10.1161/01.CIR.86.1.167>
- Yan, X., Anzai, A., Katsumata, Y., Matsubashi, T., Ito, K., Endo, J., Yamamoto, T., Takeshima, A., Shinmura, K., Shen, W., Fukuda, K., & Sano, M. (2013). Temporal dynamics of cardiac immune cell accumulation following acute myocardial infarction. *Journal of Molecular and Cellular Cardiology*, 62, 24–35. <https://doi.org/10.1016/j.yjmcc.2013.04.023>
- Yano, T., Miura, T., Ikeda, Y., Matsuda, E., Saito, K., Miki, T., Kobayashi, H., Nishino, Y., Ohtani, S., & Shimamoto, K. (2005). Intracardiac fibroblasts, but not bone marrow derived cells, are the origin of myofibroblasts in myocardial infarct repair. *Cardiovascular Pathology*, 14(5), 241–246. <https://doi.org/10.1016/j.carpath.2005.05.004>
- Yu, M., Guaraldi, M. T., Mistry, M., Kagan, M., McDonald, J. L., Drew, K., Radeke, H., Azure, M., Purohit, A., Casebier, D. S., & Robinson, S. P. (2007). BMS-747158-02: A novel PET myocardial perfusion imaging agent. *Journal of Nuclear Cardiology*, 14(6), 789–798. <https://doi.org/10.1016/j.nuclcard.2007.07.008>
- Zhao, T., Zhao, W., Chen, Y., Ahokas, R. A., & Sun, Y. (2010). Vascular Endothelial Growth Factor (VEGF)-A: Role on Cardiac Angiogenesis following Myocardial Infarction. *Microvascular Research*, 80(2), 188. <https://doi.org/10.1016/J.MVR.2010.03.014>



**UNIVERSITY  
OF TURKU**

ISBN 978-951-29-8156-4 (PRINT)  
ISBN 978-951-29-8157-1 (PDF)  
ISSN 0355-9483 (Print)  
ISSN 2343-3213 (Online)